Contribution from the Laboratorium für anorganische Chemie, Eidgenössische Technische Hochschule, Zürich, Switzerland, and Chemistry Department, South Dakota State University, Brookings, South Dakota 57006

Static and Dynamic Jahn–Teller Distortions in CuN_6 Complexes. Crystal Structures and EPR Spectra of Complexes between Copper(II) and Rigid, Tridentate *cis,cis*-1,3,5-Triaminocyclohexane (tach): $Cu(tach)_2(ClO_4)_2$, $Cu(tach)_2(NO_3)_2$. Crystal Structure of $Ni(tach)_2(NO_3)_2$

J. H. AMMETER, H. B. BÜRGI,* E. GAMP, V. MEYER-SANDRIN, and W. P. JENSEN

Received February 14, 1978

The complex cation $Cu(tach)_2^{2+}$ (tach ≡ *cis,cis*-1,3,5-triaminocyclohexane) was investigated in two different solids, $Cu(tach)_2(NO_3)_2$ and $Cu(tach)_2(ClO_4)_2$, by X-ray crystallography at room temperature and by EPR spectroscopy between 4 and 300 K. In the perchlorate salt the CuN_6 octahedron shows essentially tetragonal, static elongation between 4 and 300 K. The nitrate salt undergoes a phase transition at ~120 K; below 120 K $Cu(tach)_2^{2+}$ is statically distorted; immediately above 120 K $Cu(tach)_2^{2+}$ dynamically oscillates between two and, at higher temperatures, between all three possible, tetragonal elongations of the CuN_6 octahedron. The degree of elongation (Jahn–Teller radius R_{JT}) was estimated from the observed temperature factors of $Cu(tach)_2(NO_3)_2$ and $Ni(tach)_2(NO_3)_2$ by two methods. Both methods, namely semirigid body analysis of the entire complex cation $M(tach)_2^{2+}$ and analysis of differences in thermal motion between Cu, Ni and N, lead essentially to the same value for R_{JT} (0.33 Å). Furthermore both R_{JT} and the average Cu–N distance d_0 were found to be equal within experimental error for dynamically distorted $Cu(tach)_2(NO_3)_2$ and statically distorted $Cu(tach)_2(ClO_4)_2$. Further values of R_{JT} and values of E_{JT} (the stabilization energy gained by Jahn–Teller distortion) were obtained from literature data on CuN_6 complexes with six chemically equivalent ligand atoms ($Cu(en)_3^{2+}$, $Cu(bpy)_3^{2+}$, $Cu(phen)_3^{2+}$, $Cu(NO_2)_6^{4-}$). Comparison of all data yields strikingly similar R_{JT} (=0.32 ± 0.03 Å) and E_{JT} (=0.20 ± 0.02 μm^{-1}). This suggests that consideration of the local CuN_6 fragment alone (cluster model) provides an adequate description of the Jahn–Teller effect in octahedral Cu(II) complexed to six chemically equivalent nitrogen ligand atoms.

1. Introduction

1.1. Structure and Spectroscopy of Cu(II) Complexes. Among coordination compounds the complexes of bivalent copper have played a particularly important role for recent developments of theoretical chemistry.[1-3] There are probably two main reasons for the enormous number of structural and spectroscopic studies devoted to this class of compounds: (I) Cu(II) complexes are interesting from a purely *structural* point of view because of their "*plasticity*",[3] i.e., because of the ability of the Cu(II) center to realize—with a given set of ligands—a variety of different coordination geometries with relatively small changes in thermodynamic stability. (II) Cu(II) complexes with their single hole in the 3d shell are rewarding objects for *spectroscopic* studies as their optical and magnetic properties are more readily interpreted in terms of *electronic* properties than those of most other transition-metal compounds.[1]

The "plasticity" of Cu(II) compounds and the interpretability of their spectroscopic data taken together allow extensive correlations between changes in the electronic wave function (ψ_{el}) and changes in the molecular structure ($\vec{R}$); of course elucidation of the structure–wave function–energy relationship in molecular systems is one of the central problems of theoretical chemistry.

Particular attention has been devoted to *centrosymmetric six-coordinate* CuL_6 complexes. For these systems a theoretical model explaining (or sometimes even predicting) many remarkable structural, spectroscopic, thermodynamic, and kinetic properties was developed some 20 years ago.[4-6] On the basis of the Jahn–Teller theorem[7] the topology of the Born–Oppenheimer energy surface $E_{el}(\vec{R})$ of cubic (or trigonal) d^9 systems in the vicinity of the structure of maximum symmetry, $\vec{R}_0$, has been described in great detail. It took a long time, however, until the theory was brought in a form appropriate for direct use in interpreting experimental data.[2,8-13] The main aspects of this theoretical model[2,12,13] will be briefly summarized in the next section.

1.2. Potential Energy Surface of Octahedral Cu(II) Complexes.[2,12,13] The model for the $3N - 6 = 15$ dimensional Born–Oppenheimer surface $E_{el}(\vec{R})$ of an octahedral CuL_6 cluster is conveniently expressed in terms of the symmetry coordinates S_i of a structure with O_h symmetry. In a first crude approximation (the so-called harmonic first-order model) the dependence of E_{el} on $\vec{R}$ is assumed to be parabolic for all symmetry coordinates S_i except two, the degenerate Cu–L stretching coordinates of e_g symmetry

$$S_{2a}(e_g) = \frac{1}{\sqrt{12}}(\Delta d_1 + \Delta d_2 - 2\Delta d_3 + \Delta d_4 + \Delta d_5 - 2\Delta d_6)$$

$$S_{2b}(e_g) = \frac{1}{2}(\Delta d_1 - \Delta d_2 + \Delta d_4 - \Delta d_5) \qquad (1)$$

in which the Δd_i's measure deviations of the six individual Cu–L_i distances from the average Cu–L distance d_0. Distortions along $\pm S_{2a}$ imply tetragonally compressed and elongated coordination, respectively, while distortions along linear combinations of S_{2a} and S_{2b} in general imply orthorhombic coordination of Cu(II). In the subspace corresponding to these coordinates, the function $E_{el}(S_{2a},S_{2b})$ assumes the form of a Mexican hat (Figure 1)

$$E_{el}(|S_2|) = E_0 \pm A\cdot|S_2| + \frac{f}{2}\cdot|S_2|^2 \qquad (2)$$

where A and f are appropriate linear and quadratic force constants. In this approximation (Figure 1) a continuous set of energetically equivalent distorted structures along the circular valley

$$\vec{R}(|S_2|,\phi) = (R_{JT}\cos\phi, R_{JT}\sin\phi) \qquad (0 \le \phi \le 2\pi) \qquad (3)$$

is predicted. The valley has a radius $|S_2|$ equal to the Jahn–Teller radius R_{JT} (=A/f) and its bottom is stabilized relative to the origin by the Jahn–Teller energy E_{JT} (=$A^2/2f$).

E_{JT} and R_{JT} are related by the equation

$$E_{JT} = \frac{1}{2}\left(\frac{R_{JT}}{a}\right)^2 h\nu \qquad (4)$$

i.e., E_{JT} is proportional to the frequency ν of the radial vibration and to the square of the ratio between the Jahn–Teller dis-

* To whom correspondence should be addressed at Eidgenössische Technische Hochschule.

0020-1669/79/1318-0733$01.00/0

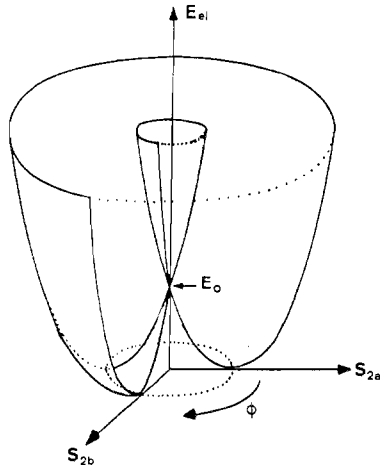

Figure 1. Two-dimensional section through the potential energy surface of a CuL_6 cluster (harmonic first-order model, eq 2) showing the dependence of the electronic energy E_{el} on the degenerate Cu–L stretching coordinates $S_{2a}(e_g)$ and $S_{2b}(e_g)$. The circular valley (dotted line at bottom of potential) with radius R_{JT} is stabilized by the Jahn–Teller energy E_{JT} relative to the energy E_0 at $S_{2a} = S_{2b} = 0$.

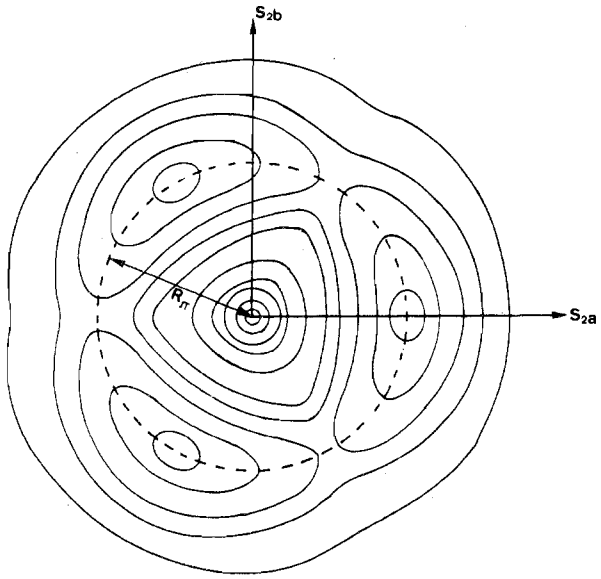

Figure 2. Contour diagram of the mexican hat potential surface showing the effects of nonlinear terms. The surface shows C_{3v} symmetry with three minima corresponding to three equivalent tetragonal elongations and with three saddle points corresponding to three equivalent tetragonal compressions of the CuL_6 cluster. A circular section of this surface along the dotted line (radius R_{JT}) is shown in Figure 3a.

tortion R_{JT} and the zero-point amplitude a. The quadratic force constant f of this vibration is

$$f = 4\pi^2\mu\nu^2 = \frac{h\nu}{a^2} = \frac{2E_{JT}}{R^2_{JT}} \qquad (5)$$

where μ is the mass of L. Note, that in this approximation only two of the four observables E_{JT}, R_{JT}, ν, and a appearing in eq 4 and 5 are independent.

In the case of large Jahn–Teller coupling higher order terms have to be included in the description of $E_{el}(\vec{R})$ in order to obtain a realistic shape of the potential in the low-energy region; the resulting surface $E_{el}(S_{2a},S_{2b})$ now shows C_{3v} symmetry, i.e., it exhibits at least three minima and three saddle points as shown in the contour diagram of Figure 2. If these additional "warping" terms are small relative to the dominant first-order term, the minima and the saddle points

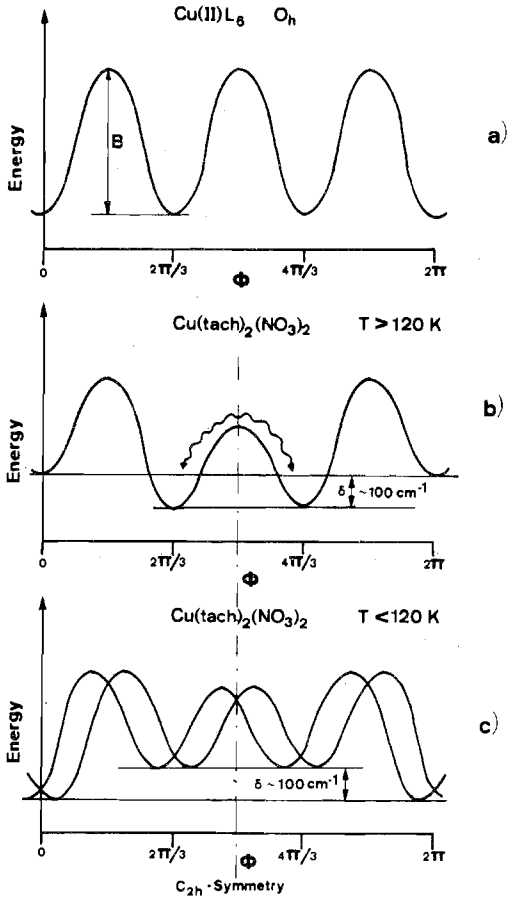

Figure 3. Schematic representation of circular sections $V(\phi)$ (eq 6) along Jahn–Teller valleys: (a) showing three equivalent minima as expected for unperturbed CuL_6 clusters (see Figure 2), (b) showing nonequivalent minima for $Cu(tach)_2(NO_3)_2$ at $T > 120$ K as expected for a CuL_6 cluster slightly perturbed by a crystalline environment of C_{2h} symmetry (the wavy line indicates the possibility of thermal transitions between the equivalent minima), (c) showing energetically nonequivalent minima for $Cu(tach)_2(NO_3)_2$ at $T < 120$ K for two CuL_6 clusters occupying two sites related by twofold symmetry.

remain approximately[2] on the original Jahn–Teller circle and the separation into a radial and an angular coordinate ($|S_2|$, ϕ) remains meaningful. In its simplest form the angular potential $V(\phi)$ at $|S_2| = R_{JT}$ can be expressed as[11]

$$V(\phi) = E_{el}(|S_2| = R_{JT};\phi) = B(1 - \cos 3\phi)/2 \qquad (6)$$

shown pictorially in Figure 3a. If both the angular barrier height B and the radial vibrational energy $h\nu$ are much smaller than the Jahn–Teller energy E_{JT}, the R_{JT},E_{JT} relationships of eq 4 and 5 remain valid and the radial rigidity of the CuL_6 cluster is still predicted to be as high as in a orbitally nondegenerate system. However, the angular flexibility would be strongly dependent on B and on temperature.

In principle all the characteristic potential constants can be investigated by various experimental methods: E_{JT} ($\simeq$2000 $cm^{-1} \simeq 6$ kcal $mol^{-1} \simeq 24$ kJ mol^{-1}) by optical spectroscopy, R_{JT} ($\simeq$0.3 Å) and a ($\simeq$0.1 Å) by diffraction experiments, B ($\simeq$300 cm^{-1}) by EPR and Raman spectroscopy, and $h\nu$ ($\simeq$400 cm^{-1}) by Raman spectroscopy. But since the theoretical model summarized above has been developed for free gaseous CuL_6 clusters only, and since these are difficult to observe experimentally, it is useful to ask in what sense the cluster model is applicable to Cu(II) complexes actually encountered in condensed phases.

1.3. Applicability Range of the Cluster Model for Cu(II) Complexes in the Solid State. In order to test whether the cluster model summarized above remains useful also for the

description of structural and spectroscopic properties of *solids* containing Cu(II) with six chemically equivalent ligand atoms L in the first coordination sphere, it is useful to distinguish between the following cases: (I) hexacoordinated Cu(II) occupying sites of cubic or trigonal symmetry in hard (ionic or covalent) lattices, (II) $Cu(lig)_n^{\nu+}$ complexes containing a cubic or trigonal CuL_6 fragment, embedded in molecular crystals and occupying sites of (a) cubic or trigonal symmetry or (b) lower symmetry.

In both classes the copper compounds may be studied either in pure form or diluted in a suitable host compound (e.g., a Zn(II) compound doped with a small fraction of Cu(II)). Diluted samples offer two important advantages relative to the stoichiometric compounds: first, the reduction of interactions between Cu centers results in optimum spectral resolution (e.g., nuclear hyperfine structure in EPR spectra); second, the shape of the effective potential energy surface $E_{el}(\vec{R})$ for individual CuL_6 clusters in a host lattice changes much less with temperature than in undiluted Cu(II) compounds, where strong cooperative structural changes occur quite frequently, particularly in class I. On the other hand detailed structural information on individual CuL_6 clusters is accessible only in undiluted compounds.

Among the diluted systems in class I, MgO,[14] CaO,[15,16,19] $Ca(OH)_2$,[17] and NaCl[18] doped with Cu(II) have been carefully investigated by EPR[14-18] and Raman[19] spectroscopy. For these systems the main limitation to the applicability of the cluster model lies in the nonexistence of a single, dominant local e_g vibrational mode, i.e., in the strong coupling of CuL_6 deformations to those of the whole lattice.[20,21] Undiluted compounds satisfying the criteria of class I are extremely rare because the cooperative forces between the strongly coupled CuL_6 clusters often induce permanent static distortions; nevertheless octahedral CuO_6 fragments showing cubic symmetry do occur in certain perovskites at sufficiently high temperatures.[22]

In contrast to compounds in class I, $Cu(lig)_n^{\nu+}$ complexes belonging to class II are only weakly coupled to the surroundings, and the assumption of a single, dominant, local Jahn–Teller-active vibrational mode is more reasonable. Well-known representatives of Cu(II) complexes with six chemically equivalent ligand atoms include complexes with six monodentate ligands, e.g., $Cu(H_2O)_6^{2+}$,[23,24] $Cu(NO_2)_6^{4-}$,[25,26] and $Cu(imid)_6^{2+}$ (imid = imidazole),[27-29] trigonal complexes with three bidentate ligands, e.g., $Cu(en_3)^{2+}$ (en = ethylenediamine),[30-33] $Cu(bpy)_3^{2+}$ (bpy = 2,2′-bipyridyl),[34-37] $Cu(phen)_3^{2+}$ (phen = 1,10-phenanthroline),[36,37] and $Cu(ompa)_3^{2+}$ (ompa = octamethylpyrophosphoramide),[39,40] and trigonal complexes with two tridentate ligands, e.g., $Cu(tach)_2^{2+}$ (tach = *cis,cis*-1,3,5-triaminocyclohexane).[41]

Since the structural and spectroscopic properties for a given type of CuL_6 cluster in class I are strongly influenced by lattice forces, no transferability of potential constants from lattice to lattice can be expected. There are good reasons to believe, however, that for class II solids the lattice forces are less determining and that the local CuL_6 energy surfaces are very similar in different crystalline or liquid environments. As a consequence approximate transferability of R_{JT}, E_{JT}, and $h\nu$ on one side and strong variations of the small angular barrier B on the other side can be expected. In class IIb solids the local energy surface $E_{el}(S_{2a},S_{2b})$ has lost its C_{3v} symmetry; the positions of the local minima along the main Jahn–Teller valley (ϕ_i) and their mutual energy differences (δ_{ij}) and barriers (B_{ij}) are no longer equivalent (see, e.g., Figure 3b,c), and again, individual behavior is expected mainly for the angular part of the potential. In general, transferability of R_{JT}, E_{JT}, and $h\nu$ should be best in the case of bulky ligands, bulky counterions, and low ionic charges.

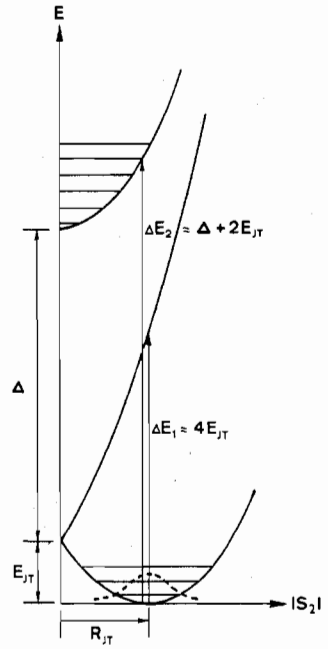

Figure 4. Planar section through the two sheets of the mexican hat potential (Figure 1) for the electronic ^2E_g ground state and also through an averaged potential curve for the $^2T_{2g}$ excited state predicting the first two optical transitions at approximately $4E_{JT}$ and $\Delta + 2E_{JT}$ (see ref 12, p 183).

The present restriction of the discussion to complexes with six equivalent ligand atoms does not imply that all the characteristic properties of strictly octahedral or trigonal Cu(II) complexes should disappear completely in analogous systems of lower symmetry. It has become increasingly clear during the last few years[2,3] that the strong topological effect of the d^9 electronic configuration on the potential energy surface is reflected in many features of the coordination chemistry of Cu(II) in general,[1,3] even though some complications enter an adequate theoretical description of complexes with nonequivalent ligand atoms in the first coordination sphere.[38]

The expectation that the local cluster potential energy surface is relatively inert against modifications by intermolecular forces and also the validity of eq 4 and 5 can be checked experimentally with the help of structural and spectroscopic data for different solids containing the same $Cu(lig)_n^{\nu+}$ complex ion.

1.4. Experimental Access to the Potential Parameters. Optical absorption spectroscopy can give approximate information on the cubic ligand field splitting Δ and also indirectly on the Jahn–Teller energy E_{JT}. For $E_{JT} >> h\nu > kT$ application of the Franck–Condon principle within the harmonic first-order model (section 1.2) predicts the center of gravity of the first d–d transition (intra-^2E_g) at

$$\Delta E_1 \simeq 4E_{JT} \tag{7}$$

and for the second d–d transition ($^2T_{2g} \leftarrow {}^2E_g$) at

$$\Delta E_2 \simeq \Delta + 2E_{JT} \tag{8}$$

if similar force constants for the active e_g vibration in both electronic states are assumed (Figure 4).[12] Both ΔE_1 and ΔE_2 should be quite insensitive to changes in the angular parameters ϕ_i, δ_{ij}, and B_{ij} as long as $E_{JT} >> B_{ij}$, δ_{ij}.

Structural analysis by X-ray, neutron, or electron diffraction gives information on the Jahn–Teller radius R_{JT}. In the case of permanent static distortion in low symmetry sites, R_{JT} is given by the equation

$$R_{JT}^2 = S_{2a}^2 + S_{2b}^2 = \sum_{i=1}^{6} \Delta d_i^2 \tag{9}$$

As in eq 1, S_{2a} and S_{2b} denote the two components of the degenerate e_g distortion and the six Δd_i's are deviations of individual Cu–L bond lengths from the average value d_0. In cases of purely dynamic or disordered static distortion (statistical occupation of the equivalent angular minima shown in Figures 2 and 3) R_{JT} is accessible from experimental Cu–L_i mean-square amplitudes of vibration $\langle \Delta d_i^2 \rangle_{JT}$

$$R_{JT}^2 = \sum_{i=1}^{6} \langle \Delta d_i^2 \rangle_{JT} = \sum_{i=1}^{6} \langle \Delta d_i^2 \rangle_{obsd} - \sum_{i=1}^{6} \langle \Delta d_i^2 \rangle_{res} \qquad (10)$$

if the Jahn–Teller contribution (JT) to the observed root-mean-square amplitudes (obsd) is much larger than the residual vibrational contributions (res) from all other Cu–L stretching modes.[8] This condition is somewhat more stringent than the one mentioned earlier, namely $R_{JT} >> a$ or $E_{JT} >> h\nu$.

An electron diffraction experiment in the gas phase yields the quantities $\langle \Delta d_i^2 \rangle_{obsd}$ directly. In an X-ray or neutron diffraction study of crystalline solids the situation is more complex, since effects of disorder, librational, and translational motion also contribute to the measured "ellipsoids of thermal motion". As will be shown, reasonable estimates for the residual contributions $\langle \Delta d_i^2 \rangle_{res}$ *not* related to the dynamic Jahn–Teller effect can be obtained from a comparison with the corresponding ellipsoids in isostructural lattices with orbitally nondegenerate metal centers such as Ni(II) or Zn(II).[30]

As in the case of the optical determination of E_{JT}, the structural determination of R_{JT} is independent of the angular parameters ϕ_i, δ_{ij}, and B_{ij} as long as $E_{JT} >> \delta_{ij}$: because eq 9 or 10 holds for any point along the Jahn–Teller circle.

EPR spectroscopy at different temperatures yields information almost exclusively on the angular potential parameters,[2,9-14,20,23,42] because the electronic ground-state wave function does depend on ϕ explicitly. For $E_{JT} >> h\nu$ the singly occupied molecular orbital $\psi(\uparrow)$ can be represented as

$$\psi(\uparrow) = \cos\frac{\phi}{2}\psi_a + \sin\frac{\phi}{2}\psi_b \qquad (11)$$

i.e., each point along the circular Jahn–Teller valley of Figures 1–3 is associated with a particular linear combination of the two degenerate e_g MO's ψ_a and ψ_b which can be written in LCAO form as

$$\begin{aligned} \psi_a &= c_M|3d_{x^2-y^2}(Cu)\rangle - c_L|\sigma_a(L)\rangle \\ \psi_b &= c_M|3d_{3z^2-r^2}(Cu)\rangle - c_L|\sigma_b(L)\rangle \end{aligned} \qquad (12)$$

$\sigma_a(L)$ and $\sigma_b(L)$ are normalized, σ-antibonding linear combinations of ligand atomic orbitals of appropriate symmetry.[43] The metal (c_M) and ligand (c_L) coefficients obey the normalizing condition $c_M^2 - 2c_Mc_LS_\sigma + c_L^2 = 1$ where S_σ is a group overlap integral. For the upper sheet of the potential surface in Figure 1, $\psi^*(\uparrow)$ is given by the orthogonal complement to $\psi(\uparrow)$.

In the case of cubic or trigonal site symmetry (class I or IIa) a superposition of three axial spectra associated with the occupation of the three equivalent minima in Figures 2 and 3a is observed[23] if the barrier B is larger than kT. For small barriers, B, a single spectrum with cubic anisotropy typical for a state fully delocalized over all three minima appears.[14] As temperature increases a gradual transition to a single averaged isotropic spectrum will eventually occur in both cases. This is due to increasing thermal population of higher angular levels. The temperature dependence of this process yields information about B.

In the case of low site symmetry (class IIb) at low temperature a single anisotropic spectrum corresponding to exclusive population of the lowest minimum is observed,[24] as long as all δ_{ij} are substantially larger than kT.[24,25] From the **g** tensor the location ϕ_1 of this minimum along the Jahn–Teller circle can be determined, since for a singly occupied orbital $\psi(\uparrow)$ (eq 11) the following first-order equations are approximately valid:[42]

$$g_1 = 2.0023 + 8u\cos^2\frac{\phi}{2} \qquad (13)$$

$$g_2 = 2.0023 + 2u\left(\cos\frac{\phi}{2} + \sqrt{3}\sin\frac{\phi}{2}\right)^2 \qquad (14)$$

$$g_3 = 2.0023 + 2u\left(\cos\frac{\phi}{2} - \sqrt{3}\sin\frac{\phi}{2}\right)^2 \qquad (15)$$

with

$$u = k(\zeta/\Delta E_2) \qquad (16)$$

Here ζ is the effective one-electron spin–orbit coupling parameter, ΔE_2 is the center of gravity of the second d–d band (eq 8), and k is an orbital reduction factor resulting from covalency. In the simplest MO model (rigid AO's, neglect of π bonding) k is equal to the Mulliken Cu $3d_\sigma$ population of the singly occupied orbital $\psi(\uparrow)$[43] (eq 11).

$$k = P_\sigma(M) = c_M^2 - c_Mc_LS_\sigma \qquad (M = Cu) \qquad (17)$$

In this approximation the average g value is independent of ϕ and given by[42]

$$g_{iso} = 2.0023 + 4u - 5u^2 \qquad (18)$$

to second order in u.

In principle, in the case of high barriers B_{ij} at higher temperatures a superposition of nonequivalent anisotropic spectra associated with Boltzmann populations of the nonequivalent local minima would be expected; however, in all known cases the barriers are relatively low and rapid vibrational relaxation leads to a single averaged spectrum.[24,25] With increasing temperature the magnitude and the orientation of the **g** tensor change due to thermal population of higher angular levels which contain larger contributions from the remaining local minima at angles ϕ_i ($i \neq 1$), separated from the lowest minimum by an energy δ_{1i}. In this case the trigonometric terms in eq 13–15 have to be replaced by their expectation values obeying the conditions

$$\left\langle \cos^2\frac{\phi}{2} \right\rangle + \left\langle \sin^2\frac{\phi}{2} \right\rangle = 1 \qquad (19)$$

$$\left\langle \left(\sin\frac{\phi}{2}\right)\left(\cos\frac{\phi}{2}\right) \right\rangle = 0 \qquad (20)$$

In the high-temperature limit ($kT >> \delta_{ij}, B_{ij}$) $\langle \cos^2(\phi/2) \rangle = \langle \sin^2(\phi/2) \rangle = {}^1/_2$ holds, and an isotropic spectrum with $g_1 = g_2 = g_3 = g_{iso}$ (eq 18) results.

It should also be mentioned that in undiluted systems exchange and magnetic dipole interactions between adjacent copper ions can complicate the interpretation of the spectra considerably.[1]

Raman spectroscopy gives information on both radial ($h\nu$) and angular potential parameters (B, δ). However, an unambiguous interpretation of Raman lines in terms of transitions between the vibrational levels of the $E_{el}(S_{2a},S_{2b})$ surface is much more difficult than interpretation of optical, diffraction, or EPR data. There is one case[19] known to the authors where a detailed assignment has been attempted.

1.5. Present Investigation. In this paper we attempt a test of the expectation formulated above, namely that for a given hexacoordinated complex $Cu(lig)_n^{\nu+}$ in different lattices all observables which are more or less independent of the angular potential parameters (d_0, R_{JT}, ΔE_1, g_{iso} and derived quantities

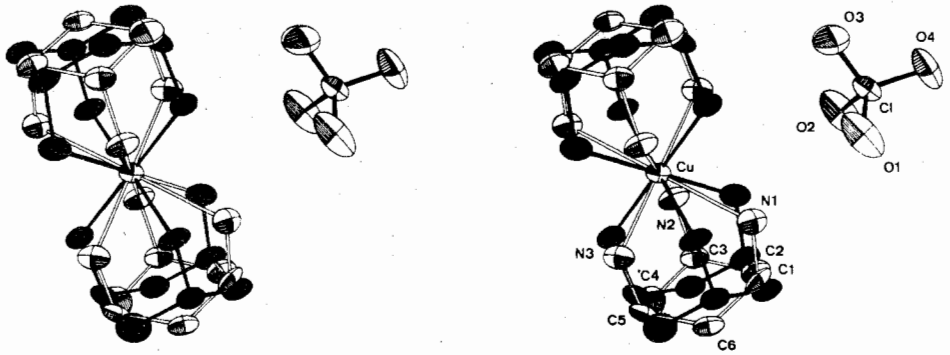

Figure 5. Stereodiagram of the disordered $Cu(tach)_2^{2+}$ ions and of a neighboring ClO_4^- ion. The black and white cations are related by a statistical mirror plane (*b,c* plane) parallel to the plane of projection. The atomic numbering corresponds to that in Table V.

such as E_{JT}, k, f) should remain approximately constant. To this end, we investigate here two different salts of a trigonal complex with a local CuN_6 chromophore, $Cu(tach)_2(ClO_4)_2$ and $Cu(tach)_2(NO_3)_2$, by X-ray crystallography at room temperature and by EPR spectroscopy between 4 and 300 K. For the nitrate salt we also analyze the corresponding isomorphous nickel(II) compound by X-ray crystallography at room temperature in order to make possible a comparison of the thermal motion ellipsoids in the MN_6 chromophore with and without Jahn–Teller effect. Finally we compare our structural and spectroscopic results with literature data on related complexes with CuN_6 chromophores.

2. Results from X-ray Analysis

2.1. Experimental Section. Bis(*cis,cis*-1,3,5-triaminocyclohexane)copper(II) Perchlorate ($Cu(tach)_2(ClO_4)_2$). Crystal data and details of data collection are given in Table I. The space group derived from photographic data is either *Cmca* or *C2ca*. *Cmca* was used in the structure analysis. Standard deviations of intensities were calculated as $\sigma(I) = (\text{peak} + 4\cdot\text{background})^{1/2} + 0.01I$ with $I = \text{peak} - 2\cdot\text{background}$.

The three-dimensional *Patterson* function shows Cu at 0, 0, 0 and 0, $^1/_2$, $^1/_2$ (site symmetry C_{2h}). A Cu-phased electron density function shows 12 nearest neighbors of the metal ion, three of which are symmetry independent. This may be interpreted in terms of two centrosymmetric $Cu(tach)_2$ cations that are disordered with respect to the crystallographic mirror plane (Figure 5). On the basis of the disordered but resolved nitrogen positions and the expected geometry of the ligand, six carbon atom positions could be estimated, but due to the disorder some of the carbon atoms overlap substantially. In order to avoid a singular or almost singular matrix of normal equations, constraints on the C–N and the C–C bond lengths were introduced into the full-matrix least-squares refinements of positional and thermal parameters and of an extinction correction (H's in calculated positions, $d(CH) = 1.0$ Å, $d(NH) = 0.9$ Å, $B_H = B_X + 2$ Å^2 where X is C or N). Two models with the same number of positional parameters but differing in the bond length constraints and the description of thermal motion were analyzed: (a) Cu, N, Cl, O anisotropic, C isotropic, d(CN) fixed at 1.48 Å using the method of undetermined multipliers, $R^a = 0.058$, $R_w^a = 0.057$; (b) Cu, N, Cl, O, C anisotropic, d(CN) fixed at 1.485 Å; d(CC) fixed at 1.527 Å, undetermined multipliers, $R^b = 0.046$, $R_w^b = 0.048$. The weighting function used was $w = \exp(1.8(\sin^2\theta)/\lambda^2)$. A Hamilton R test ($R = R^a/R^b = 0.0573/0.0483 = 1.186$ vs. $R(24, 1050, 0.005) = 1.022$) shows that model a may be strongly rejected. Positional and thermal parameters obtained from model b are given in Table II. The success of the constrained refinement may also be considered as evidence for the centrosymmetric space group *Cmca*. Most computations were performed with the X-RAY 72 system of programs, constrained refinements with a program developed locally.

Table I. Crystal Data, Details of Data Collection and Structure Solution (tach = *cis,cis*-1,3,5-Triaminocyclohexane)

	$Cu(tach)_2(ClO_4)_2$	$Cu(tach)_2(NO_3)_2$	$Ni(tach)_2(NO_3)_2$
formula	$C_{12}H_{30}N_6O_8Cl_2Cu$	$C_{12}H_{30}N_8O_6Cu$	$C_{12}H_{30}N_8O_6Ni$
mol wt	520.64	445.99	441.15
a, Å	9.68 (1)	18.496 (4)	18.369 (4)
b, Å	18.00 (2)	7.289 (2)	7.328 (2)
c, Å	12.14 (1)	7.201 (2)	7.155 (2)
β, deg	90.00 (1)	110.22 (2)	110.45 (2)
V, Å^3	2115.5	911.0	902.5
space group	*Cmca*	*C2/m*	*C2/m*
Z	4	2	2
d_c	1.635	1.618	1.623
d_x	1.64	1.62	1.62
diffractometer	Hilger & Watts Y290	Nonius CAD4	Nonius CAD4
radiation	Mo Kα[a]	Mo Kα[a]	Mo Kα[a]
scan	$2\theta/\omega$	$2\theta/\omega$[b]	$2\theta/\omega$[b]
crystal dimensions, mm	0.3 × 0.3 × 0.4	0.2 × 0.2 × 0.15	0.3 × 0.3 × 0.3
No. of observations	1155 ($F \geq \sigma(F)$)	915 ($F \geq 0.5\sigma(F)$)	998 ($F \geq 0.5\sigma(F)$)
$2\theta_{max}$, deg	54	53	53
μ, cm^{-1} (no correcn)	13.8	12.9	11.2
extinction coeff	3×10^{-7}[c]		6.5×10^{-3}
R	0.046	0.050	0.026
R_w	0.048	0.053	0.031
source of scattering factors[e]	Cu(II), ref 67; Cl(0), ref 68; C(val), N(0), O(0), ref 67; H, ref 69	Cu(0), ref 67; N(0), O(0), C(0), ref 68; H, ref 69	Ni(0), ref 67; N(0), O(0), ref 68; C(0), ref 68; H, ref 69

[a] Graphite monochromatized. [b] Variable scan speed. [c] Obtained from linear regression on the 20 most affected reflections with $(\sin\theta)/\lambda \leq 0.201$ ($\ln I_{calcd}/I_{obsd}$ vs. I_{calcd}). [d] g as obtained from XRAY 72. [e] Dispersion corrections from ref 67.

Bis(*cis,cis*-1,3,5-triaminocyclohexane)metal(II) Nitrates ($Cu(tach)_2(NO_3)_2$ and $Ni(tach)_2(NO_3)_2$). The two structures are isomorphous. Crystal data and some details of data collection and interpretation are given in Table I. Standard deviations of intensities were obtained as $\sigma^2(I) = \sigma^2(\text{peak}) + 4\sigma^2(\text{background}/2)$. The positions of all nonhydrogen atoms were found from the three-dimensional *Patterson* function. Positional and anisotropic thermal parameters were refined by full-matrix least-squares methods using unit weights and

Table II

(A) $Cu(tach)_2(ClO_4)_2$ Positional Parameters ($\times 10^4$) and Thermal Motion Tensors ($\times 10^3$) in the Form $\exp\{-2\pi^2(a^{*2}U_{11}h^2 + b^{*2}U_{22}k^2 + c^{*2}U_{33}l^2 + 2a^*b^*U_{12}hk + 2a^*c^*U_{13}hl + 2b^*c^*U_{23}hl)\}$[a]

atom	x	y	z	U_{11}	U_{22}	U_{33}	U_{12}	U_{13}	U_{23}
Cu	5000	0000	5000	32 (1)	40 (1)	65 (1)	0	0	2 (1)
N1	3892 (7)	9491 (3)	3448 (6)	52 (3)	61 (3)	89 (4)	5 (6)	−8 (6)	10 (6)
N2	6713 (6)	9398 (3)	4533 (6)	39 (3)	54 (3)	100 (5)	−1 (5)	1 (6)	−8 (6)
N3	4207 (6)	9075 (3)	5805 (6)	61 (4)	60 (3)	82 (4)	2 (6)	13 (6)	1 (6)
C1	4172 (18)	8687 (3)	3292 (9)	54 (5)	60 (6)	82 (6)	3 (8)	−20 (9)	−17 (9)
C2	5710 (16)	8526 (7)	3147 (10)	69 (7)	53 (4)	90 (7)	7 (11)	1 (12)	−8 (11)
C3	6549 (9)	8608 (3)	4206 (8)	43 (4)	54 (4)	98 (6)	2 (8)	4 (8)	−14 (10)
C4	5928 (11)	8156 (5)	5149 (9)	57 (5)	50 (5)	102 (8)	12 (19)	−10 (10)	−12 (9)
C5	4398 (9)	8320 (4)	5336 (9)	68 (6)	42 (4)	83 (6)	−5 (8)	1 (9)	13 (8)
C6	3588 (9)	8247 (4)	4262 (8)	45 (4)	52 (4)	110 (7)	−7 (8)	2 (9)	−12 (10)
Cl	0000	0951 (1)	3828 (1)	51 (1)	63 (1)	82 (1)	0	0	−15 (2)
O1	1140 (4)	0525 (3)	3539 (5)	76 (2)	179 (4)	187 (5)	47 (6)	3 (6)	−50 (8)
O3	0000	1574 (4)	3156 (6)	360 (14)	79 (4)	128 (6)	0	0	7 (8)
O4	0000	1178 (4)	4932 (5)	171 (7)	156 (6)	90 (4)	0	0	−35 (8)

(B) Calculated Hydrogen Atom Coordinates ($\times 10^4$) and Isotropic Thermal Parameters ($\times 10^4$) for $Cu(tach)_2(ClO_4)_2$

atom	x	y	z	U, Å²	atom	x	y	z	U, Å²
HN11	2973	9549	3527	911	H22	5826	8003	2862	1023
HN12	4178	9735	2844	911	H3	7518	8435	4053	787
HN21	7097	9642	3960	887	H41	6454	8274	5829	1023
HN22	7300	9403	5107	887	H42	6032	7617	4964	1023
HN31	4585	9072	6485	874	H5	4028	7954	5895	1023
HN32	3289	9148	5865	874	H61	2628	8428	4404	1092
H1	3675	8547	2613	1023	H62	3566	7711	4058	1092
H21	6095	8877	2571	1023					

[a] Standard deviations in units of last significant figure in parentheses.

Table III

(A) $Cu(tach)_2(NO_3)_2$ Positional Parameters ($\times 10^4$) and Thermal Motion Tensors ($\times 10^4$) in the Form $\exp\{-2\pi^2(a^{*2}U_{11}h^2 + b^{*2}U_{22}k^2 + c^{*2}U_{33}l^2 + 2a^*b^*U_{12}hk + 2a^*c^*U_{13}hl + 2b^*c^*U_{23}kl)\}$[a]

atom	x	y	z	U_{11}	U_{22}	U_{33}	U_{12}	U_{13}	U_{23}
Cu	5000	5000	0	248 (4)	322 (5)	287 (5)	0	84 (3)	0
N1	5935 (3)	5000	−1177 (7)	418 (27)	476 (30)	304 (24)	0	55 (20)	0
N2	5654 (2)	2907 (5)	2014 (5)	340 (16)	429 (20)	480 (19)	−72 (15)	162 (14)	−37 (17)
C1	6739 (3)	5000	238 (8)	288 (26)	492 (35)	364 (29)	0	149 (22)	0
C2	6901 (2)	3272 (6)	1522 (6)	314 (18)	435 (24)	435 (21)	80 (17)	132 (16)	−1 (19)
C3	6493 (2)	3242 (6)	3029 (6)	289 (17)	387 (22)	391 (20)	46 (16)	77 (15)	54 (17)
C4	6628 (3)	5000	4243 (8)	349 (28)	444 (33)	317 (27)	0	88 (23)	0
N3	4193 (3)	0	2880 (8)	351 (25)	444 (30)	442 (28)	0	111 (21)	0
O1	4393 (3)	0	1385 (7)	676 (30)	451 (26)	573 (30)	0	371 (24)	0
O2	4098 (3)	1464 (6)	3593 (6)	1485 (41)	698 (28)	690 (25)	442 (29)	519 (26)	−43 (22)

(B) Calculated Hydrogen Coordinates ($\times 10^4$) and Isotropic Thermal Parameters ($\times 10^4$) for $Cu(tach)_2(NO_3)_2$

atom	x	y	z	U, Å²	atom	x	y	z	U, Å²
H1	7086	5000	−605	760	H42	6268	5000	5039	760
H21	7482	3163	2237	760	HN1	5833	3857	−2087	760
H22	6720	2155	593	760	HN21	5387	2800	3036	760
H3	6702	2151	3983	760	HN22	5561	1712	1205	760
H41	7187	5000	5191	760					

[a] Standard deviations in units of last significant figure in parentheses.

hydrogens in calculated positions (d(CH) = 1.02 Å, d(NH) = 1.02 Å, B_H = 6 Å²). Results are found in Tables III and IV. For all computations the X-RAY 72 system of programs was used.

2.2. Discussion of the Molecular Structures. The tridentate tach ligands are coordinated facially to the metal ions which show octahedral coordination with differing degrees of distortion. Bond lengths, bond angles, and torsion angles for anions and cations are given in Table V.

The ions $Cu(tach)_2^{2+}$ and $Ni(tach)_2^{2+}$ in the *nitrate salts* show C_{2h} site symmetry and also approximate D_{3d} symmetry. Some of the deviations from approximate D_{3d} symmetry are significant; for example, one intraligand NMN angle is ~90° and the other two are ~86°. Other deviations are not significant; for example the differences between the two crystallographically independent M–N distances (a set of two distances in the crystallographic mirror plane and another of four distances in general positions) are 0.009 (7) Å for Cu and 0.003 (4) Å for Ni. Due to static Jahn–Teller distortion, $Cu^{II}N_6$ complexes usually show unequal Cu–N distances; the equal distances found here may be discussed in terms of dynamic or disordered static Jahn–Teller distortion. These possibilities will be analyzed later in conjunction with the thermal motion parameters and the EPR data. For Ni(II) the result is in accord with the expectation of regular octahedral coordination. In each complex the set of four nitrogen atoms in general positions is coplanar because of symmetry; the NMN bond angles in this plane are not significantly different from 90°. The two metal–nitrogen bonds in the crystallographic mirror plane are not orthogonal to the other four as seen from the corresponding NMN angles within a ligand, 85.7 (1) and 86.5 (1)°, respectively. The average

Table IV

(A) $Ni(tach)_2(NO_3)_2$ Positional Parameters ($\times 10^4$) and Thermal Motion Tensor ($\times 10^4$) in the Form $\exp\{-2\pi^2(a^{*2}U_{11}h^2 + b^{*2}U_{22}k^2 + c^{*2}U_{33}l^2 + 2a^*b^*U_{12}hk + 2a^*c^*U_{13}hl + 2b^*c^*U_{33}kl)\}$[a]

atom	x	y	z	U_{11}	U_{22}	U_{33}	U_{12}	U_{13}	U_{23}
Ni	5000	5000	0	190 (2)	220 (3)	202 (2)	0	71 (2)	0
N1	5914 (3)	5000	−1188 (3)	244 (11)	331 (13)	238 (11)	0	101 (9)	0
N2	5645 (1)	2942 (2)	2008 (2)	236 (7)	272 (9)	289 (8)	−6 (7)	70 (6)	41 (7)
C1	6733 (2)	5000	226 (4)	222 (13)	375 (16)	305 (14)	0	133 (11)	0
C2	6903 (1)	3290 (3)	1509 (3)	246 (9)	356 (11)	361 (10)	63 (8)	109 (8)	0 (9)
C3	6492 (1)	3251 (3)	3039 (3)	235 (9)	309 (10)	282 (9)	33 (8)	58 (7)	56 (8)
C4	6634 (2)	5000	4261 (4)	259 (13)	404 (17)	229 (13)	0	41 (11)	0
N3	4196 (1)	0	2860 (4)	317 (12)	336 (14)	324 (13)	0	101 (10)	0
O1	4392 (1)	0	1359 (3)	558 (14)	392 (13)	421 (13)	0	287 (11)	0
O2	4100 (1)	1464 (3)	3595 (3)	1129 (17)	490 (12)	543 (11)	251 (12)	423 (12)	−42 (9)

(B) Calculated Hydrogen Coordinates ($\times 10^4$) and Isotropic Thermal Parameters ($\times 10^4$) for $Ni(tach)_2(NO_3)_2$

atom	x	y	z	U, Å^2	atom	x	y	z	U, Å^2
H1	7069	5000	−641	760	H42	6270	5000	5053	760
H21	7491	3213	2261	760	HN1	5833	3883	−2087	760
H22	6730	2178	606	760	HN21	5381	2835	3044	760
H3	6699	2181	3983	760	HN22	5550	1762	1190	760
H41	7196	5000	5203	760					

[a] Standard deviations in units of last significant figure in parentheses.

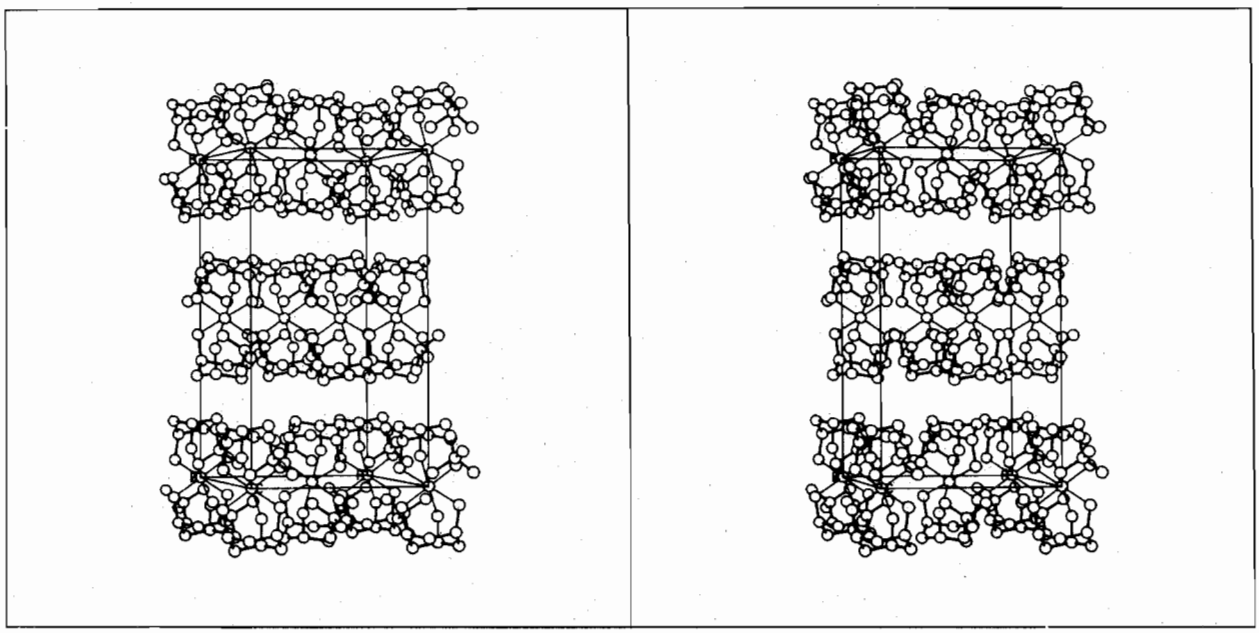

Figure 6. Stereodiagram of molecular packing in $Cu(tach)_2(ClO_4)_2$ showing layers containing $Cu(tach)_2^{2+}$ and ClO_4^- ions. Contacts between layers are through weak H···H van der Waals contacts. The viewing direction is approximately down the *c* axis; the *a* axis runs from left to right and the *b* axis from bottom to top. For clarity only one-half of the disordered $Cu(tach)_2^{2+}$ ions are shown.

torsion angles in the carbon ring are 50.5 and 51.4°, respectively; i.e., the rings are flatter than in similar cyclohexane derivatives (53–57°).[44] As a consequence the angles at carbon are relatively large, 114.2 and 114.1°, respectively, at the methylene carbon atoms, and 110.9 and 110.7°, respectively, at the ternary carbon atoms.

Strain in the torsion angles as well as in the bond angles at carbon and nitrogen of an $M(tach)_2^{2+}$ cannot be relieved easily because, for fixed bond lengths *d*(CC), *d*(CN), and *d*(MN), not all bond angles and torsion angles are independent parameters and the diminution of strain in some angles will increase strain in others. The structure of tach in its triaxial conformation not complexed to a metal ion is not available; the structure for the thermodynamically more stable triequatorial conformer has been determined in the form of $tach(HBr)_3$.[45]

The crystallographic symmetry of $Cu(tach)_2^{2+}$ in the *perchlorate salt* is C_i. Each ligand is bonded to Cu through two nitrogen atoms at short distance (average 2.07 Å) and one at large distance (2.35 Å) as expected for a d^9 cation (but contrary to the result found for $Cu(tach)_2(NO_3)_2$). From eq 9 the Jahn–Teller radius is calculated to be 0.328 Å. The average Cu–N separation d_0 in the perchlorate is 2.164 Å, the same as in the nitrate salt where it is 2.167 Å. The CuNC angles at nitrogen atoms forming short bonds are 120°, ~2° larger than those found in the nitrate salt; the bond angle at the other nitrogen is 113.5°, ~4° smaller than in the nitrate salt. The deviations of the intraligand NCuN bond angles from 90° are almost the same in the nitrate and perchlorate salts: 0.3 (1)° for one angle, 3.3° to 6.0 (2)° for the other two. The average nonbonded N···N separations are practically equal in the two compounds: 2.984 and 2.982 Å, respectively. The constraint of the CN and CC bond lengths to equal values biases the structure of the ligand toward D_{3d} symmetry and it is difficult to decide whether the deviations from approximate D_{3d} symmetry observed in the bond angles of the ligand are really significant. In the perchlorate salt the average bond angles at the methylene groups are 113.9° and at the ternary

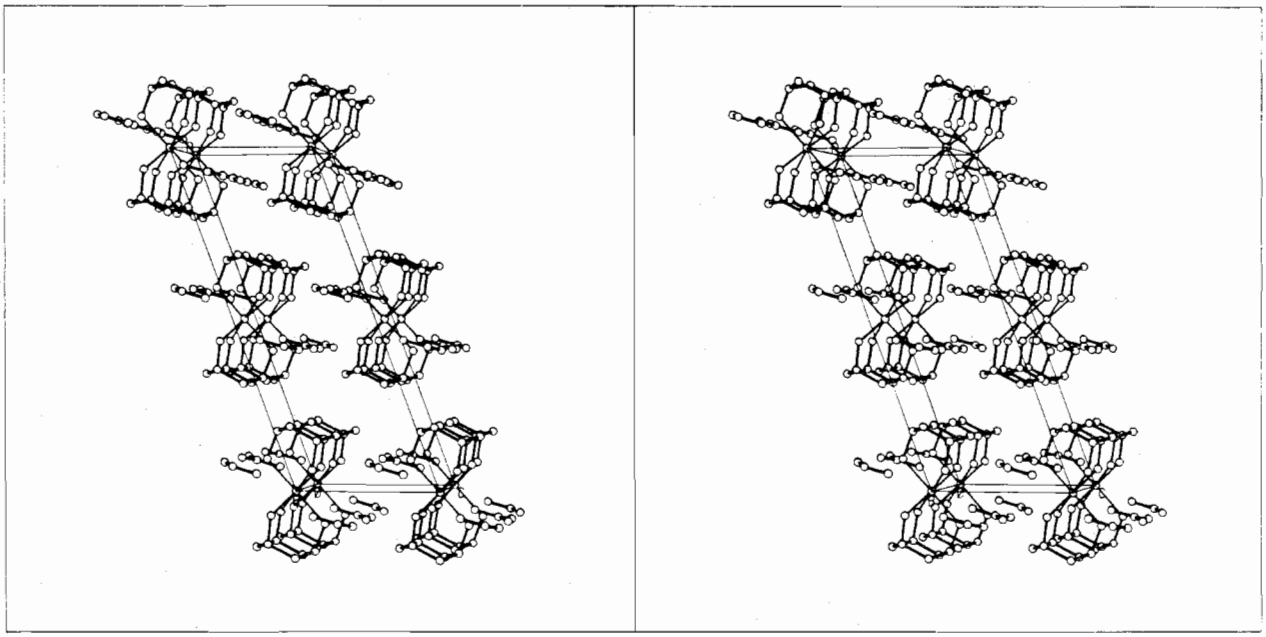

Figure 7. Stereodiagram of molecular packing in $Cu(tach)_2(NO_3)_2$ and in isostructural $Ni(tach)_2(NO_3)_2$. The viewing direction is approximately down the *b* axis; the *a* axis runs from bottom to top and the *c* axis from left to right. The $M(tach)_2^{2+}$ and NO_3^- ions are arranged in layers that are parallel to the *b*,*c* plane. Contacts between layers are through weak H···H van der Waals contacts.

carbon atoms are 110.9°, both very similar to the angles found in the nitrate salt.

2.3. Thermal Motion Parameters. As pointed out before, the six amine nitrogen atoms in $Cu(tach)_2(NO_3)_2$ are equidistant from Cu(II). The complex cation must therefore show dynamic or disordered static Jahn–Teller distortion that should manifest itself in the thermal motion parameters of the atoms.[8] Analysis of these parameters was guided by several lines of thought. First, we inspected the thermal motion parameters of individual nitrogen atoms and found significant differences with respect to size and orientation of the thermal ellipsoids in the Cu and the Ni compound. Then, because coordinated tach is likely to be fairly rigid, we analyzed sets of atomic thermal motion tensors in $M(tach)_2^{2+}$ simultaneously in terms of librational and translational oscillations of a rigid or semirigid complex cation.[46] In the analysis of thermal motion of $Cu(tach)_2^{2+}$, we found it necessary to introduce a special degree of freedom, a librational oscillation of the ligand relative to Cu(II) (semirigid model). The extra oscillation is interpreted as a manifestation of dynamic or disordered static Jahn–Teller distortion in the Cu compound. It was not needed in the analysis of $Ni(tach)_2^{2+}$ (rigid model). Third, we wanted to compare the results of the semirigid body analysis to alternative ways of analyzing for Jahn–Teller distortion amplitudes. One way of doing this is to make use of the differences ΔU(M–N) in atomic mean-square displacements U(M) and U(N) along M–N bonds. Jahn–Teller distortions derived from semirigid body analysis and from ΔU's were compared to that shown by the statically distorted $Cu(tach)_2(ClO_4)_2$ and found to be in remarkable agreement. Finally we extended thermal motion analysis to literature data of other Cu(II) complexes with six chemically equivalent nitrogen ligand atoms and again found close agreement between Jahn–Teller distortions derived from ΔU(M–N)'s and from statically distorted complexes.

The square root of eigenvalues and corresponding principal axes for observed thermal motion tensors of N1, N2, and M in $Cu(tach)_2(NO_3)_2$ and $Ni(tach)_2(NO_3)_2$ are given in Table VI. The first value listed for every nitrogen atom, $U_{11}^{1/2}$, is associated with a principal axis approximately parallel to the MN bond, the second one, $U_{22}^{1/2}$, with a principal axis that is orthogonal to the plane formed by the NM bond and the approximate threefold axis of $M(tach)_2^{2+}$, and the third one, $U_{33}^{1/2}$, with a principal axis which is orthogonal to the first two (Table VI and Figure 8). On the whole the thermal motion of the nitrogen atoms is in the usual range; it is somewhat larger in the Cu compound than in the Ni compound. As far as individual U_{ii}'s, of nitrogen are concerned, significant differences are observed between the two compounds: in $Cu(tach)_2^{2+}$ the amplitude of motion along the MN bond, $U_{11}^{1/2}$, is a maximum; in $Ni(tach)_2^{2+}$ it is a minimum. This difference implies an enhanced flexibility of the Cu–N bond relative to that of the Ni–N bond. It is compatible with the presence of dynamic or disordered static Jahn–Teller distortion in the copper complex. $U_{22}^{1/2}$ is associated with motion of the nitrogen atoms that corresponds to librational oscillations of the complex as a whole (or the ligand alone) around the approximate threefold axis (Figure 8); $U_{22}^{1/2}$ is quite large in both complexes. $U_{33}^{1/2}$ is associated with changes of the angle between the M–N bond and the approximate threefold axis; it is relatively small for both nitrogen atoms in both complexes.

Similar findings have been reported by Cullen and Lingafelter[30] for the nitrogen atoms in $Cu(en)_3SO_4$ and the corresponding Ni compound. They found that the eigenvector associated with the largest $U_{ii}^{1/2}$'s (0.232 Å for Cu(II), 0.186 Å for Ni(II)) forms an angle of 19.1° with the Cu–N bond but of 94.5° with the Ni–N bond.

2.3.1. Interpretation of Thermal Motion Parameters in Terms of Rigid or Semirigid Body Motion of $Cu(tach)_2^{2+}$. Since we expected tach to be fairly rigid, we attempted to describe its thermal motion in terms of librations and translational oscillations of a rigid body expressed in the form of three tensors **T**, **L**, and **S**.[46a] **T** and **L** describe the translational and librational oscillations, respectively, and **S** describes the coupling between the two. The elements of **T**, **L**, and **S** are obtained from the observed thermal parameters of carbon and nitrogen atoms through a least-squares procedure (weights $w = \sigma^{-2}(U_{obsd})$). The quality of the fit between observed thermal parameters, U_{obsd}, and those calculated from **T**, **L**, and **S**, U_{calcd}, is expressed in terms of a root-mean-square deviation, $\{[\sum w(U_{obsd} - U_{calcd})^2](\text{observations})/[(\sum w)(\text{observations} - \text{parameters})]\}^{1/2}$, and compared to $\langle\sigma(U_{obsd})\rangle$ in Table VII (sum or average over all tensor components of all

Table V. Interatomic Distances (Å) and Angles (deg)[a]

	$[Cu(tach)_2](ClO_4)_2$	$[Cu(tach)_2](NO_3)_2$	$[Ni(tach)_2](NO_3)_2$
M–N1	2.353 (7)	2.173 (6)	2.131 (3)
M–N2	2.061 (6)	2.164 (3)	2.134 (2)
M–N3	2.078 (6)		
N1–C1	1.485[b]	1.484 (6)	1.491 (3)
N2–C3		1.488 (4)	1.488 (2)
C1–C2	1.527[b]	1.529 (5)	1.520 (3)
C2–C3		1.522 (6)	1.532 (3)
C3–C4		1.522 (5)	1.522 (3)
N1···N2	3.037 (9)	2.950 (6)	2.922 (3)
N1···N3	2.973 (10)		
N2···N3(N2′)	2.936 (9)	3.052 (5)	3.016 (2)
N1–M–N2	86.7 (2)	85.7 (1)	86.5 (1)
N1–M–N3	84.0 (2)		
N2–M–N3(N2′)	90.3 (2)	89.7 (1)	89.9 (1)
M–N1–C1	113.5 (6)	118.4 (4)	118.6 (2)
M–N2–C3	119.4 (5)	117.4 (3)	117.7 (1)
M–N3–C5	120.5 (6)		
N1–C1–C2	112.2 (10)	110.8 (3)	110.8 (1)
N1–C1–C6	109.8 (9)		
N2–C3–C2	112.0 (7)	110.0 (3)	109.8 (1)
N2–C3–C4	110.7 (7)	110.9 (4)	110.6 (2)
N3–C5–C4	110.8 (7)		
N3–C5–C6	109.9 (7)		
C2–C1–C6(C2′)	110.6 (9)	110.9 (4)	111.0 (2)
C1–C2–C3	113.8 (10)	113.6 (4)	113.5 (2)
C2–C3–C4	111.6 (8)	112.0 (4)	111.5 (2)
C3–C4–C5(C3′)	113.0 (8)	114.7 (4)	114.7 (2)
C4–C5–C6	110.8 (8)		
C5–C6–C1	115.0 (8)		
M N1 C1 C2	−59.6	−61.8	−61.9
M N1 C1 C6	63.8		
M N2 C3 C2	66.0	65.6	64.7
M N2 C3 C4	−59.3	−58.8	−58.8
M N3 C5 C4	55.7		
M N3 C5 C6	−67.1		
C1 C2 C3 C4	52.6	50.8	51.1
C2 C3 C4 C5 (C3′)	−53.0	−48.9	−49.3
C3 C4 C5 C6	52.1		
C4 C5 C6 C1	−51.8		
C5 C6 C1 C2	50.8		
C3 C2 C1 C6 (C2′)	−50.7	−52.5	−53.4
Cl–O1	1.389 (5)		
Cl–O3	1.387 (7)		
Cl–O4	1.401 (7)		
O1–Cl–O3	107.4 (3)		
O1–Cl–O4	113.6 (3)		
O3–Cl–O4	109.0 (4)		
N–O1		1.253 (8)	1.248 (4)
N–O2		1.223 (5)	1.234 (3)
O1–N–O2		119.2 (3)	119.6 (2)
O2–N–O2′		121.6 (6)	120.7 (3)

[a] For the nitrate salts primed and unprimed atoms are related by the molecular mirror plane. [b] Constrained values; see experimental part.

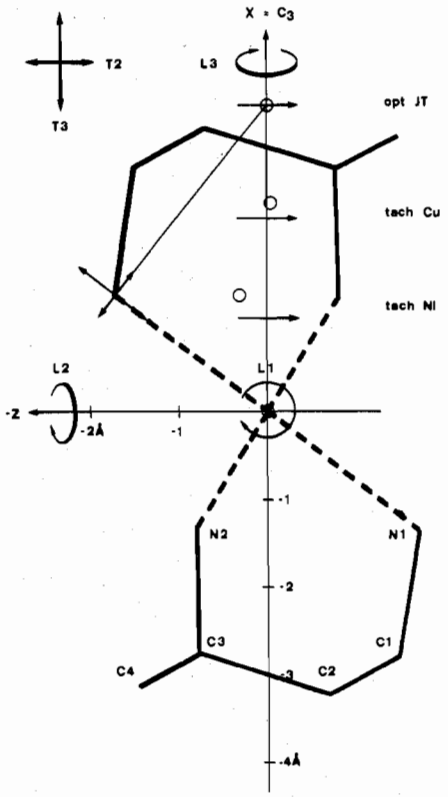

Figure 8. Results from various analyses of $Cu(tach)_2(NO_3)_2$ and $Ni(tach)_2(NO_3)_2$ thermal motion parameters. *X*, *Y*, *Z* are the inertial axes of $M(tach)_2^{2+}$ where X coincides with the approximate threefold axis of the cation and Y (perpendicular to the plane of projection) coincides with the crystallographic twofold axis. T1, T2, and T3 indicate approximate directions of translational oscillations. L1, L2, and L3 indicate approximate directions of libration axes in rigid $Ni(tach)_2^{2+}$ and semirigid $Cu(tach)_2^{2+}$. Circle and arrow labeled "opt JT" show the assumed positions of the nonrigid libration axes NRL1 and NRL2, respectively, that optimally express the effects of Jahn–Teller distortion (see Table IX). Circles and arrows labeled "tach Cu" and "tach Ni", respectively, show the positions of the ligand libration axes L1 and L2 calculated from the thermal motion parameters of the ligand alone (Table VIII). The crossed arrows at N1 indicate the effect of the libration L1 (arrow perpendicular to the Cu–N1 bond) and of the libration NRL1 (circle labeled opt JT; arrow along the Cu–N1 bond).

atoms). It is seen that for both compounds the fit of tach alone (Table VII, line 1) is as good as or better than can be expected on the basis of $\langle\sigma(U_{obsd})\rangle$ (Table VII, line 4) implying that the ligands may indeed be considered as rigid bodies. The characteristics of the respective motions are different for the Cu and Ni compound and will be described below.

One could take the alternative point of view that the metal and the two ligands constitute a complex and that the whole complex might behave as a rigid body. Because of its C_{2h} symmetry the model of a rigid $M(tach)_2^{2+}$ unit requires only two tensors, **T** and **L**, to describe rigid body motion.[46a] In spite of the increased number of observations (due to the inclusion of the metal atom in the analysis) and of the decreased number of variables (due to higher symmetry) the quality of the fit for $Ni(tach)_2^{2+}$ (Table VII, line 2) is essentially the same as before, implying that the $Ni(tach)_2^{2+}$ as a whole may be considered to be rigid. For $Cu(tach)_2^{2+}$, however, the fit has become significantly worse and this complex cannot be considered rigid. We have therefore relaxed the rigidity by introducing two additional degrees of freedom, namely, librations of the ligand relative to the metal about two orthogonal axes perpendicular to the approximate threefold axis and at distance of 3.57 Å from the metal. The distance was chosen such as to maximize the effect of this libration on the Cu–N bond lengths (opt JT, Figure 8). Table VII (line 3) shows that the root-mean-square deviation for the semirigid model of $Cu(tach)_2^{2+}$ is reduced compared to that of the rigid model. As will be discussed later the extra motion may be interpreted as a manifestation of dynamic or disordered static Jahn–Teller distortion.

We shall now discuss the models that were found to satisfactorily account for observed thermal motion parameters. Details of the motion performed by the *rigid tach* ligands alone are listed in Table VIII. Translational oscillations of the ligand in the copper complex are found to be slightly higher than those in the nickel complex, but they take place along the same directions in both complexes. The amplitudes are smallest in the direction of the approximate threefold axis, somewhat larger and practically isotropic perpendicular to it (in agreement with observed approximate C_{3v} symmetry).

Table VI. Square Root of Eigenvalues ($U_{ii}^{1/2}$) and Principal Axes of Observed Thermal Motion Tensors U for N1, N2, and M in the Inertial Axes System of $M(tach)_2^{2+}$; Angles γ between Principal Axes and M-N Bond Vectors (left $Cu(tach)_2(NO_3)_2$, right $Ni(tach)_2(NO_3)_2$)

	$U_{ii}^{1/2}$,[a] Å	X	Y	Z	γ, deg	$U_{ii}^{1/2}$,[a] Å	X	Y	Z	γ, deg
N1	0.221	0.688	0.0	−0.726	5.3	0.147	0.341	0.0	−0.940	17.6
	0.218	0.0	1.0	0.0	90	0.182	0.0	1.0	0.0	90
	0.170	0.726	0.0	0.688	84.7	0.159	0.940	0.0	0.341	72.4
N2	0.224	0.562	−0.549	0.619	16.6	0.153	0.972	−0.199	0.127	39.8[b]
	0.209	−0.076	0.710	0.700	73.6	0.185	0.009	0.566	0.824	89.8
	0.171	0.824	0.440	−0.357	87.1	0.155	0.236	0.800	−0.552	50.6[b]
	0.179	0.0	1.0	0.0		0.148	0.0	1.0	0.0	
	0.171	0.136	0.0	0.991		0.142	0.520	0.0	0.854	
	0.157	0.991	0.0	−0.136		0.137	0.854	0.0	−0.520	

Direction Cosines of M-N Bond Vectors

M-N1	0.618	0.0	−0.786	0.610	0.0	−0.793
M-N2	0.601	−0.705	0.377	0.596	−0.707	0.381

Transformation Matrix from Fractional Coordinates x, y, z to Inertial Coordinates X, Y, Z (in Å)

$$\begin{bmatrix} X \\ Y \\ Z \end{bmatrix} = \begin{bmatrix} 15.955\ 16 & 0.0 & 1.271\ 12 \\ 0.0 & 7.289\ 00 & 0.0 \\ -9.356\ 00 & 0.0 & 7.087\ 92 \end{bmatrix} \begin{bmatrix} x \\ y \\ z \end{bmatrix} \qquad \begin{bmatrix} X \\ Y \\ Z \end{bmatrix} = \begin{bmatrix} 15.830\ 23 & 0.0 & 1.246\ 29 \\ 0.0 & 7.328\ 00 & 0.0 \\ -9.317\ 94 & 0.0 & 7.045\ 93 \end{bmatrix} \begin{bmatrix} x \\ y \\ z \end{bmatrix}$$

[a] For every atom listed $i = 1$–3. [b] Approximately degenerated eigenvalues; direction of eigenvectors in arbitrary.

Table VII. Root-Mean-Square Deviations between Observed and Calculated Thermal Motion Parameters for Various Rigid Body Models

model	rms deviation, Å		no. of observations	no. of parameters varied
	Cu(II)	Ni(II)		
rigid tach	0.0017	0.0009	30	12
rigid $M(tach)_2^{2+}$	0.0031	0.0010	34	8
semirigid $M(tach)_2^{2+}$ [a]	0.0014	0.0008	34	10
$\langle\sigma(U_{obsd})\rangle$[b]	0.0023	0.0010		

[a] Including two extra librations with respect to two orthogonal axes perpendicular to the approximate threefold axis at 3.57 Å from the metal. [b] Experimental standard deviation averaged over all tensor components of all atoms in an $M(tach)_2^{2+}$ unit.

Table VIII. Results of Thermal Motion Analysis of the Ligand Alone in the Inertial Axis System of the Ligand (Cu, Left; Ni, Right; Compare Figure 8)

Amplitudes of Libration and Direction Cosines of Corresponding Libration Axes

	X	Y	Z		X	Y	Z
L1 = 4.3°	0.0	1.0	0.0	L1 = 2.7°	0.0	1.0	0.0
L2 = 4.2°	0.068	0.0	0.998	L2 = 2.6°	−0.157	0.0	0.988
L3 = 3.0°	0.998	0.0	−0.068	L3 = 3.5°	0.988	0.0	0.157

Displacements Δ of Libration Axes L*i* from Origin of Inertial Frame Measured along L*i*[46a] (These Are Approximately Parallel to Inertial Axis System)

	L1, Å	L2, Å	L3, Å		L1, Å	L2, Å	L3, Å
Δ(L1)	0.0	0.039	0.011	Δ(L1)	0.0	0.300	−0.982
Δ(L2)	0.0	0.0	−0.185	Δ(L2)	0.0	0.0	−1.292
Δ(L3)	0.0	0.219	0.0	Δ(L3)	0.0	0.095	0.0

Amplitudes of Translational Oscillation, Reduced to Correspond to Nonintersecting Axes Description in the Inertial Axis System[46a] and Direction Cosines of Corresponding Translation Directions

	X	Y	Z		X	Y	Z
T1 = 0.191 Å	0.0	1.0	0.0	T1 = 0.164 Å	0.0	1.0	0.0
T2 = 0.182 Å	0.160	0.0	0.987	T2 = 0.155 Å	0.257	0.0	0.966
T3 = 0.140 Å	0.987	0.0	−0.160	T3 = 0.136 Å	0.966	0.0	−0.257

Transformation Matrices from Crystal System to Inertial Axis System

$$\begin{bmatrix} X \\ Y \\ Z \end{bmatrix} = \begin{bmatrix} 15.790\ 91 & 0.0 & 1.393\ 55 \\ 0.0 & 7.289\ 00 & 0.0 \\ -9.630\ 63 & 0.0 & 7.064\ 87 \end{bmatrix} \begin{bmatrix} x \\ y \\ z \end{bmatrix} \qquad \begin{bmatrix} X \\ Y \\ Z \end{bmatrix} = \begin{bmatrix} 15.682\ 16 & 0.0 & 1.356\ 63 \\ 0.0 & 7.328\ 00 & 0.0 \\ -9.565\ 04 & 0.0 & 7.025\ 52 \end{bmatrix} \begin{bmatrix} x \\ y \\ z \end{bmatrix}$$

Origin of Crystal System in the Inertial Axis System

0.037 27	0.0	−2.370 97	0.033 40	0.0	−2.342 81

Translational motion of the ligands is closely similar to the thermal motion of the metals alone (Tables VI and VIII; ref 47). This seems physically meaningful since it implies that, as far as translational motion is concerned, the complexes $M(tach)_2^{2+}$ may be considered as a whole (see below). Librational motion of the ligands, like translational, is isotropic perpendicular to the approximate threefold axis; i.e., it also conforms to the approximate C_{3v} molecular symmetry. The respective amplitudes L1 and L2 are smaller than L3 for the nickel compound and larger than L3 for the copper compound (Table VIII); i.e., L1 and L2 deviate in opposite directions from L3 the amplitude of libration about the approximate

Table IX. Results of Thermal Motion Analysis of Semirigid $Cu(tach)^{2+}$ (Left) and Rigid $Ni(tach)_2^{2+}$ (Right) in the Corresponding Inertial Axis Systems (X, Y, Z): Amplitudes of Libration, Li, and of Ligand Libration Relative to the Metal, NRLi; Amplitudes of Translational Oscillation, Ti; Direction Cosines of Corresponding Libration Axes and Translation Directions (Compare Figure 8)

	X	Y	Z		X	Y	Z
L1 = 1.7 °	0.0	1.0	0.0	L2 = 1.8 °	0.0	1.0	0.0
L2 = 1.8 °	0.273	0.0	−0.962	L2 = 1.9 °	0.008	0.0	1.000
L3 = 2.4 °	0.962	0.0	0.273	L3 = 3.4 °	1.000	0.0	−0.008
NRL1 = 2.8 °	0.0	1.0	0.0[a]				
NRL2 = 2.5 °	0.0	0.0	1.0[a,b]				
T1 = 0.179 Å	0.0	1.0	0.0	T1 = 0.148 Å	0.0	1.0	0.0
T2 = 0.171 Å	0.200	0.0	0.980	T2 = 0.143 Å	0.738	0.0	0.675[c]
T3 = 0.158 Å	0.980	0.0	−0.200	T3 = 0.138 Å	0.675	0.0	−0.738[c]

[a] Distance of the libration axis from the origin equal to 3.57 Å. [b] Direction of eigenvector not refined. [c] Approximately degenerate eigenvalues, direction of eigenvectors is arbitrary.

threefold axis which is similar in both compounds (3.0–3.5°).

Differences in librational amplitudes and in particular their effects on atomic motion are meaningful only in connection with the position of the respective axes relative to a specified molecular coordinate system. In the present case the crystallographic symmetry of the ligand alone is only C_s and therefore the positions of the three librational axes with respect to the molecular coordinate system of inertia are variable parameters of the rigid body model (hidden in S^{46a}). These positions are given in terms of displacements Δ from the center of mass of the ligands (Table VIII). In the copper complex the Δ's do not exceed 0.22 Å. Thus, in terms of this model, the ligand may be considered to librate essentially about its center of mass. In the nickel complex, however, Δ's amount to as much as −1.0 and −1.3 Å along the approximate threefold axis.

The direction of the displacements is toward the nickel atom which sits 2.34 Å from the center of mass of the ligand. If, for the moment being, we make the simplifying assumption that M is at rest, we can easily see that librations of tach with amplitudes L1 and L2 affect M–N distances more for the Cu than for the Ni compound. This is because in the Cu compound the corresponding libration axes (Figure 8, tach Cu) are closer to the pivot point for which the effect of libration on M–N distances is maximized (Figure 8, opt JT), whereas for the Ni compound these axes (Figure 8, tach Ni) are closer to the pivot point for which the effect of libration on M–N bonds vanishes (Figure 8, L1). These findings agree with expectations based on the Jahn–Teller effect.

Some results for the second and third model (rigid $Ni(tach)_2^{2+}$ and semirigid $Cu(tach)_2^{2+}$) are given in Table IX. For the nickel compound the thermal motion may be described in terms of a major rigid body libration about the approximate threefold axis of the complex and two minor librations perpendicular to the major one. By symmetry the libration axes are constrained to pass through the metal atom, and librational motion therefore does not affect the NiN bond lengths to first order. Translational motion is almost isotropic and, because of the weights used in the least-squares calculation, determined mainly by the motion of the Ni atom. This model represents the simplest description of the thermal motion of $Ni(tach)_2^{2+}$ that yields satisfactory agreement between U_{obsd} and U_{calcd} (Table VII). Contrary to $Ni(tach)_2^{2+}$, the simplest model to satisfactorily describe thermal motion of $Cu(tach)_2^{2+}$ requires libration of the ligands relative to copper (NRL) in addition to translation (T) and overall libration (L). For this model the L tensor was nevertheless found to be very similar to that of rigid $Ni(tach)_2^{2+}$ (Table IX).

The additional oscillations of the ligand (NRL) are reasonably well resolved from the rigid body libration (L1, L2), the correlation coefficients being about −0.4. Because the ligands move relative to the Cu atom, changes of the Cu–N bond lengths are induced. The oscillation with amplitude NRL1, for example, increases d(Cu–N1) while it decreases d(Cu–N2) and vice versa (Figure 8). If we assume that bond distances related by the crystallographic center of symmetry lengthen or shorten simultaneously, we may interpret the motions of the ligands relative to the copper as being due to a dynamic Jahn–Teller effect or to a superposition of approximately equal amounts of three static structures, each one elongated along a different direction of the coordination octahedron. The root-mean-square changes $\langle \Delta d_i^2 \rangle^{1/2}$ of the Cu–N distances are calculated from NRL1 and NRL2 as 0.136 and 0.128 Å, respectively.

We have also tested the dependence of the above results on the position of the extra ligand libration axes relative to the metal atom since this position is not fixed by symmetry. It was found that the contributions to the thermal amplitudes from NRL1 and NRL2 were insensitive to this parameter in the range investigated (2.0–4.5 Å for the distance between the metal atom and the libration axes, Figure 8). In this whole range the root-mean-square deviation between U_{obsd} and U_{calcd} is smaller than the estimated average experimental uncertainty $\langle \sigma(U_{obsd}) \rangle$ of 0.0023 Å^3 (Table VII) and from this we conclude that, while our data require more freedom of motion than available to rigid $Cu(tach)_2^{2+}$, they do not permit determining accurately the position of the extra libration axes introduced to account for the Jahn–Teller effect.

2.3.2. Jahn–Teller Distortions from Individual Atom Temperature Factors and from the Statically Distorted $Cu(tach)_2(ClO_4)$. We have also analyzed the thermal motion parameters of metal and nitrogen atoms alone (Table VI) by evaluating the atomic mean-square displacements along the direction of the connecting M–N bond. In the case of copper the difference between these two quantities, $\Delta U(Cu–N_i) = U(N_i) - U(Cu) = \langle \Delta d_i^2 \rangle_{obsd}$, the mean-square amplitude of the copper–nitrogen stretching motion, is composed of contributions from all Cu–N stretching vibrations, Jahn–Teller active and inactive ones (eq 10). In order to single out the contributions from the Jahn–Teller inactive vibrations (res), we have assumed that $\langle \Delta d_i^2 \rangle_{res} \approx \Delta U(Ni–N_i)$ and have estimated the Jahn–Teller contribution as

$$\langle \Delta d_i^2 \rangle_{JT} = \Delta U(Cu–N_i) - \Delta U(Ni–N_i) \qquad (21)$$

The result ($\langle \Delta d_1^2 \rangle^{1/2} = 0.137$ (13), $\langle \Delta d_2^2 \rangle^{1/2} = 0.133$ (10) Å) is similar to the result obtained from semirigid body analysis (0.136, 0.128 Å) described in detail in the preceding section. The agreement is not quite trivial since the result from semirigid body analysis depends on the U's of all atoms of the complex cation, whereas the result described above depends only on the U's of Cu and N.

Having determined $\langle \Delta d_i^2 \rangle$ for dynamically distorted $Cu(tach)_2^{2+}$ we now turn to the question of comparing R_{JT} in the dynamically distorted nitrate salt and the statically distorted perchlorate salt. The Jahn–Teller radii

$$R_{JT} = \{\sum_{i=1}^{6} \langle \Delta d_i^2 \rangle\}^{1/2} \qquad (10')$$

Table X. Static and Dynamic Jahn-Teller Distortion Amplitudes of CuN_6 Complexes Derived from X-ray Diffraction Data

crystal	S[a]	$\Delta U^{1/2}$(Ni-N_i)[b]	$\Delta U^{1/2}$(Cu-N_i)[b]	$\langle\Delta d^2$(Cu-N_i)$\rangle_{JT}^{1/2}$ [c]	d_0(Ni-N)[d]	d_0(Cu-N)[d]
$M(tach)_2(NO_3)_2$[e]	C_{2h} 1	0.052 (12)	0.147 (12)	0.137 (13) d	2.132 (3)	2.170 (5)
	C_{2h} 2	0.052 (9)	0.143 (8)	0.133 (10) d		
$Cu(tach)_2(ClO_4)_2$[e]	C_i 1		0.095 (21)			
	C_i 2		0.136 (18)	0.134 (6) s		2.164 (6)
	C_i 3		0.151 (12)			
$M(en)_3SO_4$[30,48]	D_3	0.097 (16)	0.176 (5)	0.146 (12) d	2.124 (6)	2.150 (2)
$Cu(bpy)_3(ClO_4)_2$[49]	C_1			0.145 (7) s		2.134 (7)
$Cu(phen)_3(ClO_4)_2$[50]	C_1			0.137 (13) s		2.134 (13)
$K_2PbM(NO_2)_6$[51-53]	T_h	0.047 (10)	0.144 (7)	0.136 (8) d	2.080 (2)	2.111 (4)
			0.125 (3)[f]	0.116 (8) d		2.114 (5)[f]
$Tl_2PbCu(NO_2)_6$[54]	T_h		0.126	d		2.118 (6)
$Rb_2PbCu(NO_2)_6$[55]	D_{2h} 1		0.062 (23)			
	D_{2h} 2		0.145 (16)	0.103 (7) sd		2.136 (5)
	D_{2h} 3		0.147 (15)			
$Cs_2PbCu(NO_2)_6$[56]	D_{2h} 1		0.036 (20)			
	D_{2h} 2		0.188 (24)	0.140 (5) sd		2.171 (7)
	D_{2h} 3		0.165 (19)			
$K_2CaCu(NO_2)_6$[57]	D_{2h} 1		0.067 (4)			
	D_{2h} 2		0.040 (7)	0.124 (1) s		2.138 (1)
	D_{2h} 3		0.059 (4)			
$K_2SrM(NO_2)_6$[58]	D_{2h} 1		−0.030 (22)[g]			
	D_{2h} 2	0.047 (11)	0.040 (16)	0.130 (2) s	2.078 (1)	2.127 (2)
	D_{2h} 3		0.053 (12)			
$K_2BaM(NO_2)_6$[59,60]	D_{2h} 1		0.060 (9)			
	D_{2h} 2	0.045 (9)	0.025 (20)	0.126 (2) s	2.080 (2)	2.132 (2)
	D_{2h} 3		0.043 (12)			

[a] Site symmetry and numbering of crystallographically inequivalent nitrogen atoms N_i. [b] $\Delta U^{1/2}(M\text{-}N_i) = (U(N_i) - U(M))^{1/2}$ in Å, evaluated along M-N_i bonds. [c] Cu-N_i Jahn-Teller distortion amplitudes $\langle\Delta d_i^2\rangle^{1/2} = R_{JT}/6^{1/2}$, in Å estimated from thermal motion parameters of dynamically distorted CuN_6 octahedra (d) or from structural data of statically (s) and partially dynamically (sd) distorted CuN_6 octahedra. In the case of partially dynamic distortions R_{JT} was obtained from the average (d_0) and the short (d_{min}) Cu-N distance as $R_{JT} = 2(3^{1/2})(d_0 - d_{min})$. [d] Average M-N bond distances in Å. [e] This work. [f] Neutron diffraction data. [g] Negative sign indicates negative difference $U(N_i) - U(M)$.

obtained above from two analyses of thermal motion (0.329 and 0.320 Å) agree very closely with the radius

$$R_{JT} = \{\sum_{i=1}^{6} \Delta d_i^2\}^{1/2} \qquad (9')$$

calculated from static distortion (0.328 Å). This confirms the expectation formulated in the introduction, namely, that for $Cu(tach)_2^{2+}$ in different lattices R_{JT} should remain approximately constant.

2.4. Jahn–Teller Distortion for Other CuN_6 Systems. In order to get a better feeling for the significance of this result we applied the above procedure to all structural data available in the literature on statically and dynamically distorted Cu(II) complexes and on corresponding Ni(II) complexes with six chemically equivalent nitrogen atoms in an approximately regular octahedral arrangement. Individual Jahn–Teller Cu–N_i root-mean-square amplitudes $\langle\Delta d_i^2\rangle_{JT}^{1/2}$ were calculated from thermal motion parameters in the case of dynamically (d) distorted CuN_6 octahedra or from structural data in the case of statically (s) or partially dynamically (sd)[56] distorted CuN_6 octahedra. They are listed in Table X together with average M–N distances d_0.

Jahn–Teller distortion amplitudes for $Cu(NO_2)_6^{4-}$ in seven different lattices are all in the range 0.12 ± 0.02 Å and do not depend on whether the distortions are dynamic (d), static–dynamic (sd),[56] or static (s); individual averages are 0.126 (d), 0.121 (sd) and 0.127 (s). From this observation it would seem, as in the case of $Cu(tach)_2^{2+}$, that the cluster model described in the introduction is applicable, i.e., the radial topology of the Mexican hat surface $E_{el}(|S_2|)$ is determined mainly by the nature of the ligand NO_2^- and is perturbed only to a minor extent by the intermolecular forces of individual lattices. The total range of $\langle\Delta d_i^2\rangle_{JT}^{1/2}$ observed for the $Cu(NO_2)_6^{4-}$ chromophore in different lattices (0.103–0.140 Å) is larger than the range observed for $\langle\Delta d_i^2\rangle_{JT}^{1/2}$ of all other compounds (0.133–0.146 Å), and there is no significant difference between the average of $\langle\Delta d_i^2\rangle_{JT}^{1/2}$ for $Cu(NO_2)_6^{4-}$ (0.125 (13) Å) and the average of $\langle\Delta d_i^2\rangle_{JT}^{1/2}$ for the other compounds (0.139 (6) Å): $\langle\Delta d_i^2\rangle_{JT}^{1/2}$ is thus the same for complexes with aliphatic amines, nitrogen heterocycles and N-bonded nitrite as ligands. All types of compounds considered here may therefore be described using very similar Jahn–Teller radii R_{JT} and possibly also very similar Jahn–Teller energies E_{JT} (see section 4, below).

It may also be noted that the average Ni–N and Cu–N bond lengths d_0 remain approximately constant throughout Table X (last two columns). A possible exception is $Cu(NO_2)_6^{4-}$ ions where average bond lengths for statically distorted complexes are somewhat higher than for purely dynamically distorted structures. This could indicate a small admixture of the totally symmetric a_{1g} Cu–N breathing mode to the prevalent e_g distortion. The observation of approximately constant d_0 does of course not hold for CuN_4N_2' complexes (with chemically nonequivalent ligand atoms) where d_0 is generally larger and covers a wide range of values.[1,3] Also listed in Table X are values of $\Delta U^{1/2}$(Ni–N_i) which cluster at ~0.05 Å. This is in good agreement with the value calculated from the experimental force field of $Ni(NH_3)_6^{2+}$.[64] $\Delta U^{1/2}$(Cu–N_i)'s not affected by dynamic Jahn–Teller distortion are about the same, ~0.05 Å, while those affected are ~0.15 Å. Exceptions to this rule are $Ni(en)_3SO_4$ which shows disorder of the anion and $Cu(tach)_2(ClO_4)$ which shows disorder of the cation.

The uncertainties quoted in Table X have been obtained from the esd's in positional and thermal atomic parameters. The influence of systematic error is likely to be small for Cu–N bond lengths but is not very transparent for the atomic thermal motion parameters U_{obsd}. The thermal motion tensors obtained from X-ray diffraction will depend not only on the treatment of data (corrections for absorption and extinction) but also on the model used to fit the experimental data. The scattering curves, for example, may be chosen as those of M(II) or M(0) and for disordered structures (e.g., $Cu(tach)_2(ClO_4)_2$ or $Cu(en)_3SO_4$) it is often difficult to find an appropriate model for the electron density function. Many errors and uncertainties are likely to cancel out, however, in the process of estimating Jahn–Teller distortion amplitudes. Absorption

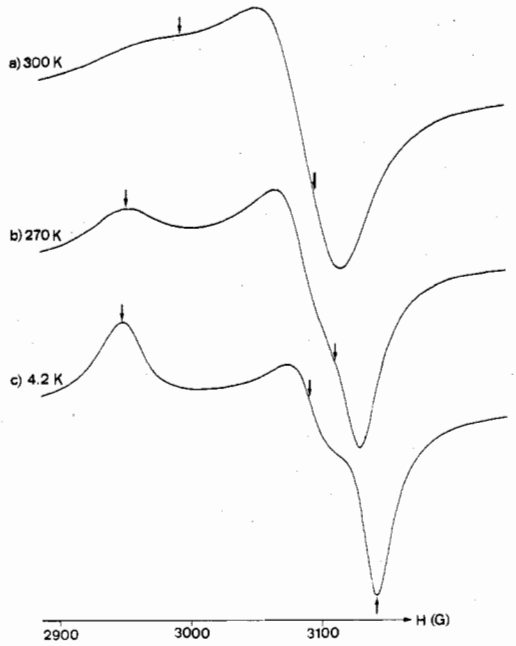

Figure 9. Temperature dependence of the X-band EPR powder spectrum of undiluted $Cu(tach)_2(ClO_4)_2$ (ν = 9.092 GHz). The arrows indicate resonance fields corresponding to approximate g_{eff} values given in the text.

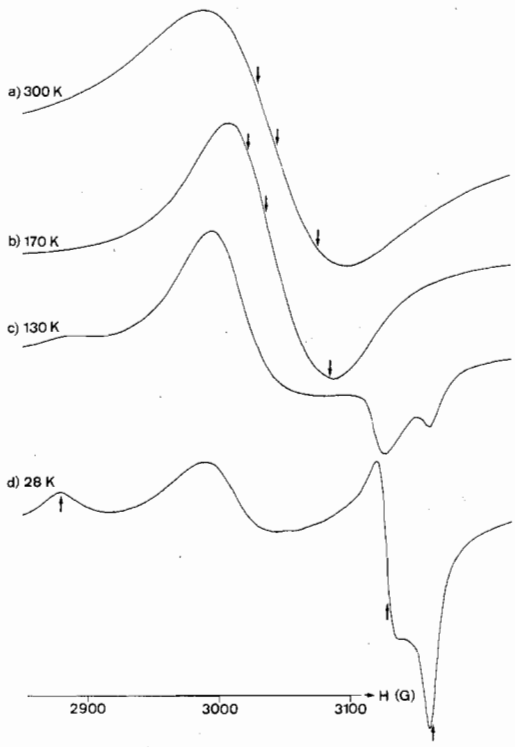

Figure 10. Temperature dependence of the X-band EPR powder spectrum of undiluted $Cu(tach)_2(NO_3)_2$ (ν = 9.085 GHz). The arrows indicate resonance fields corresponding to the g values obtained from a single-crystal analysis (Table XI). The broad peak in the center of spectrum d was not observed in the single-crystal spectrum (Figure 11) and is discussed in the text.

errors, for example, affect $U(M)$ and $U(N)$ similarly and tend to cancel for the difference $\Delta U = U(M) - U(N)$. Similarly, cancellation of the effects due to scattering curves may be expected if the same charge is assumed for both the copper and the nickel atom. In the two isostructural compounds $Cu(en)_3SO_4$ and $Ni(en)_3SO_4$, the distribution of the disordered sulfate ion is reported to be similar. For both compounds ΔU's

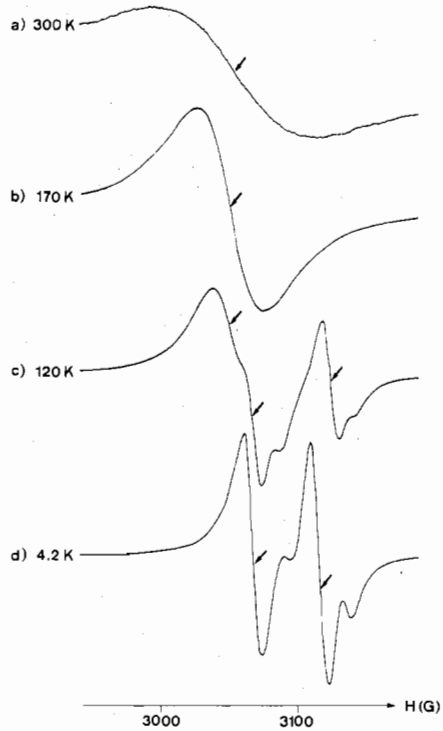

Figure 11. Temperature dependence of the X-band EPR spectrum of an undiluted $Cu(tach)_2(NO_3)_2$ single crystal in a selected orientation (magnetic field approximately parallel to one of the Cu–N2 axes). The high-temperature spectra (a) and (b) show only one signal, and the low-temperature spectrum (d) shows two main signals (arrows) and two small peaks while spectrum (c) is essentially a superposition of the spectra (b) and (d). The small peaks in spectra (c) and (d) that are without arrows originate from a second, smaller crystal attached to the main crystal. The orientation of the smaller fragment differs from that of the larger one.

tend to be high whereas the Jahn–Teller distortion amplitude—estimated as the difference between the ΔU's—lies within the range observed for the other compounds. For these reasons we believe that results from thermal motion analysis represent meaningful estimates of Jahn–Teller distortion amplitudes $\langle d^2 \rangle_{JT}^{1/2}$ in spite of many sources of systematic error.

All interpretations of thermal motion parameters in terms of dynamic or disordered static Jahn–Teller distortions rely on the assumption that Cu–N bonds related by a center of symmetry shorten or lengthen simultaneously. Since information on the phases of atomic motions in the crystal cannot be obtained from X-ray or neutron diffraction experiments, we have looked for EPR spectroscopic evidence to support our interpretation of thermal motion data.

3. Results from EPR Spectroscopy

3.1. Description of Spectra. EPR spectra of $Cu(tach)_2^{2+}$ have been recorded earlier by Childers, Wentworth, and Zompa.[41] The magnetic parameters at 80 K obtained from a polycrystalline sample of $Cu(tach)_2^{2+}$ diluted in $Zn(tach)_2(ClO_4)_2$ ($g_\parallel$ = 2.25, $g_\perp$ = 2.05, $A_\parallel = 1.76 \times 10^{-4}$, $A_\perp \leq 15 \times 10^{-4}$ cm^{-1}) were in the range expected for a tetragonally elongated CuN_6 complex.

We have now investigated undiluted polycrystalline samples of both $Cu(tach)_2(ClO_4)_2$ and $Cu(tach)_2(NO_3)_2$ between 4 and 300 K. In addition, complete single-crystal studies have been performed for the perchlorate salt at room temperature and for the nitrate salt between 4 and 300 K. The temperature dependence of the powder spectra is shown in Figures 9 and 10; that of the nitrate single-crystal spectrum for a selected crystal orientation is shown in Figure 11. In the lower temperature range both the nitrate and the perchlorate salt

Table XI. Principal Values and Reorientation of g Tensor and Line Width Tensor for $Cu(tach)_2(NO_3)_2$ at Temperatures between 4 and 300 K

T, K	g_1	g_2	g_3	g_{iso}	ΔH_1	ΔH_2	ΔH_3	α,[a] deg
4–120	2.250 (2)	2.081 (2)[b]	2.047 (2)[b]	2.126 (2)	24	(10–15)	(10–15)	
120	2.171 (4)	2.154 (3)	2.068 (3)	2.131 (3)	30	33	15	24 (3)
140	2.166 (3)	2.153 (3)	2.072 (3)	2.130 (3)	50	36	31	28 (3)
160	2.162 (4)	2.148 (3)	2.086 (3)	2.132 (3)	54	42	36	28 (4)
170	2.159 (3)	2.147 (3)	2.091 (3)	2.132 (3)	55	51	41	27 (5)
190	2.151 (4)	2.140 (4)	2.103 (3)	2.131 (4)	57	66	55	33 (5)
210	2.147 (4)	2.140 (4)	2.108 (4)	2.132 (4)	63	66	64	44 (5)
230	2.143 (5)	2.142 (4)	2.111 (4)	2.132 (4)	67	78	79	51 (5)
250	2.141 (6)	2.143 (5)	2.114 (5)	2.133 (5)	72	83	92	55 (5)
270	2.138 (6)	2.145 (5)	2.117 (5)	2.133 (5)	80	93	111	61 (5)
300	2.138 (7)	2.145 (6)	2.113 (6)	2.132 (6)	96	108	148	65 (10)

[a] Angle between g_3 axis of high-temperature tensor and g_1 axis of the low-temperature tensor in the mirror plane of the crystal (see Figure 13). [b] The second low-temperature site has the g_2 and g_3 axes interchanged.

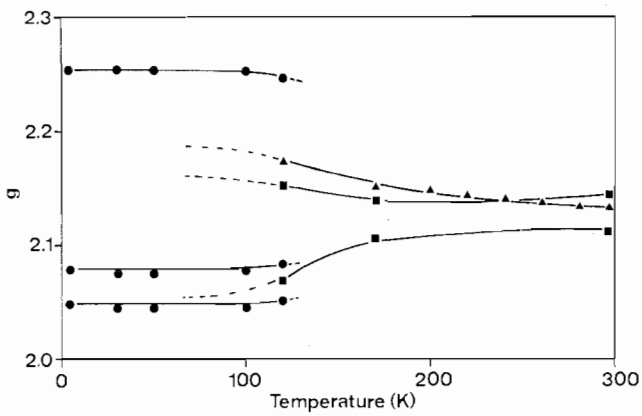

Figure 12. Temperature dependence of the principal g values in $Cu(tach)_2(NO_3)_2$. Filled circles: g_1, g_2, and g_3 values of low-temperature spectrum; corresponding principal axes coincide approximately with the three CuN directions. Filled triangles: g_2 value of high-temperature spectrum with principal axis along the twofold axis of the crystal. Filled squares: g_1 and g_3 values of high-temperature spectrum with principal axes in the mirror plane of the crystal (see Table XI and Figure 13). Solid lines refer to dominant spectra; broken lines to weak additional spectra.

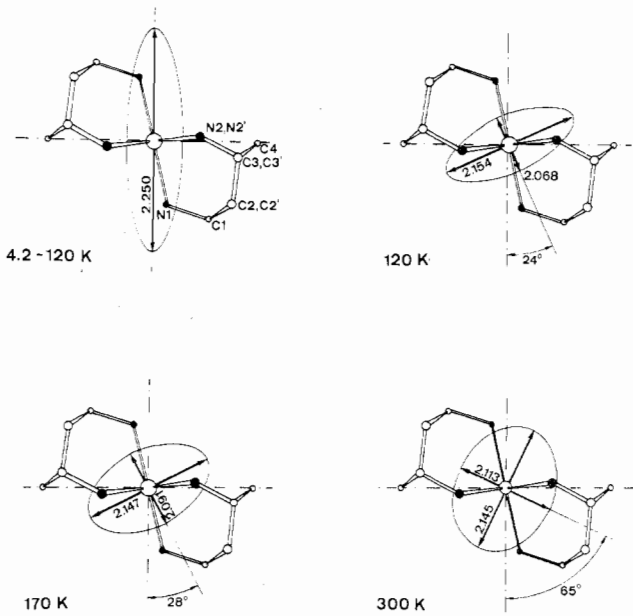

Figure 13. Shape and orientation (relative to the molecular framework) of the **g** tensor ellipsoid at various temperatures. The projection is onto the crystallographic mirror plane and shows the angle α between the g_3 principal axis of the high-temperature tensor and the g_1 principal axis (vertical dot-dash line) of the low-temperature tensor (see Table XI).

show anisotropies characteristic for statically distorted CuN_6 octahedra; at higher temperatures the total anisotropies ($g_{max} - g_{min}$) are reduced. As expected[1,42] both compounds do not exhibit copper hyperfine splittings indicating spin superexchange between adjacent molecules to be faster than ~1 GHz. The results of our EPR analyses can be summarized as follows.

$Cu(tach)_2(ClO_4)_2$. Both the shape and the effective g values (g_a = 2.203 (4), g_b = 2.100 (10), g_c = 2.061 (4), g_{iso} = 2.121) of the powder spectrum recorded at 4 K (see Figure 9) are typical for statically distorted CuN_6 octahedra with different orientations coupled by exchange interactions sufficiently strong (≥1 GHz) to average out individual Zeeman anisotropies and copper hyperfine interactions. Since the $Cu(tach)_2^{2+}$ ions in the observed crystal structure occur in four distinguishable orientations, there are several possibilities for exchange averaging (e.g., between two or between all four orientations). For reasons of molecular packing which will be discussed later, we assume exchange between two symmetry-related sites; the angle between the corresponding principal axes associated with g_1 can then be determined from the effective g values of $Cu(tach)_2(ClO_4)_2$ at 4 K, provided the molecular **g** tensor is either axially symmetric or known approximately from diluted samples.[1] Using the **g** tensor of $Cu(tach)_2^{2+}$ diluted in $Zn(tach)_2(ClO_4)_2$[41] or the similar **g** tensor of undiluted $Cu(tach)_2(NO_3)_2$ at 4 K (Table XI, first row, discussion below) we obtain an angle of 61 ± 4°. An interpretation of the low-temperature spectrum in terms of exchange interactions is also consistent with the fact that the perchlorate spectrum cannot be reproduced by computer simulation assuming a single line width parameter (effect of line width variation in exchange-coupled systems[1,42]).

Toward higher temperatures the total anisotropy of the apparent **g** tensor (arrows in Figure 9) seems to decrease somewhat: at room temperature a single crystal of $Cu(tach)_2(ClO_4)_2$ showed effective g values of g_a = 2.190 (3), g_b = 2.106 (3), and g_c = 2.086 (3) and a single line at all orientations with anisotropic line width. Consistent with our X-ray results there is no transition to an isotropic spectrum between 4 and 300 K.

$Cu(tach)_2(NO_3)_2$. The results obtained for the nitrate salt turned out to be much more informative than those for the perchlorate salt in that a gradual transition from static to dynamic behavior could be followed in detail. The temperature variation of the g values can be visualized most conveniently from the powder spectra shown in Figure 10 and from the g vs. temperature plot in Figure 12. More accurate g values and information on principal axis orientations obtained from a full single-crystal analysis at four discrete temperatures (Figure 11) are given in Table XI and Figure 13, respectively.

In the low-temperature range (4–120 K) both powder and single-crystal spectra exhibit only minor variations. Contrary to the perchlorate case, the observed **g** tensor (Table XI, first row) agrees quite well with the result obtained at 80 K by Childers et al.[41] for $Cu(tach)_2^{2+}$ diluted in $Zn(tach)_2(ClO_4)_2$

and can be attributed to a single tetragonally elongated CuN_6 octahedron with a slight orthorhombic deformation.[1] From eq 13–15 it follows that the electronic ground state is characterized by a singly occupied $d_{x^2-y^2}$ orbital with a slight admixture of $d_{3z^2-r^2}$. In addition to the regular anisotropic powder pattern which could be reproduced by computer simulation using the single-crystal g values, the powder spectrum (Figure 10) showed an additional peak corresponding approximately to the average g value g_{iso}. Similar observations have been made in earlier EPR investigations of octahedral Cu(II) complexes and have been attributed to structural changes caused by the grinding process during the preparation of powdered samples.[61] Here this point will not be discussed further.

At low temperature the single-crystal analysis revealed the presence of two chemically equivalent sites. The directions of the g_1 principal axes (corresponding to the largest principal g value) are the same in both sites. The g_2 principal axis of one site coincides with the g_3 principal axis of the other and vice versa. Comparison of the principal axis directions with the room-temperature structure (Figure 13) revealed that the common g_1 axis is situated in the mirror plane of the crystal and deviates by only about 5° from the normal to the plane spanned by the four symmetry-equivalent N2 atoms. The g_2 and g_3 axes both make an angle of about 45° with the twofold axis of the crystal and coincide with the CuN2 and CuN2′ vectors, respectively, within experimental error. From this result we conclude that below 120 K the CuN_6 octahedra are statically elongated along the CuN1 direction. The small orthorhombic distortions in the two chemically equivalent sites are interrelated by the twofold axis of the room temperature structure and the space average over both orientations conforms to the overall symmetry of the crystal found at room temperature by X-ray analysis. The distinguishability of the two sites indicates slow exchange ($J < 1$ GHz) between $Cu(tach)_2^{2+}$ ions with nonidentical orientation of the g_2 and g_3 principal axes whereas the lack of copper hyperfine splitting indicates fast exchange ($J > 1$ GHz) between $Cu(tach)_2^{2+}$ ions with identical orientations.

Upon warming of the system above 120 K the low-temperature spectrum described above disappears and instead a high-temperature spectrum with reduced g anisotropy appears indicative of a phase transition around this temperature (Figures 10–13). The single-crystal EPR analysis revealed only *one* line above 120 K at all orientations. Also, the orientation of the magnetic axes at high temperature differed from that at low temperature: In the range between 120 and 300 K one axis of the **g** tensor (g_1, Table XI) coincides with the twofold axis of the crystal, while the other two (g_2, g_3), those lying in the mirror plane, gradually rotate around the twofold axis upon warming (Table XI and Figure 13). The **g** tensor observed in the high-temperature spectrum at 120 K (Table XI) may be interpreted as average of two tensors related by the crystallographic twofold axis with g values the same as in the low-temperature spectrum but with the two g_1 principal axes oriented approximately along the CuN2 and CuN2′ directions, respectively (rather than along the CuN1 direction as in the low-temperature spectrum). The smallest g value (g_3) is now approximately along the CuN1 bond. At still higher temperatures the **g** tensor anisotropy diminishes gradually (Figure 12). The phase transition at ~120 K is not sharp; high-temperature and low-temperature signals coexist over a considerable range (Figure 12); also, their intensities were found to depend somewhat on the history of the temperature variation.

3.2. Structural Implications. Probable Nature of Disorder in $Cu(tach)_2(ClO_4)_2$. It was mentioned earlier that $Cu(tach)_2^{2+}$ in the perchlorate salt is disordered with respect to the crystallographic mirror plane (plane of projection in Figure 5). A model of the disorder will now be developed on the basis of the molecular packing: Figure 6 shows that the crystal structure is built of layers extending in the *ac* plane. Within a layer the cations and anions are held together through hydrogen bonds. Cohesion between successive layers along *b*, however, depends entirely on weak H···H van der Waals contacts. This anisotropy in the cohesive forces led us to consider a model of disorder with an ordered arrangement of molecules within a layer, but two alternative modes of stacking successive layers. As a consequence of the observed effective space group symmetry, successive ordered layers may be related to each other either by a twofold screw axis along *b* or alternatively by a *c* glide plane perpendicular to *b*. Both arrangements must occur in a random fashion but with comparable probability. There are two different possibilities for an ordered arrangement in the *ac* plane as well. Either the molecules at 0, 0, 0 and $^1/_2$, 0, $^1/_2$ are related by a twofold axis along *b* or by an *a* glide plane perpendicular to *c* (Figure 6). H···H contacts do not favor either of the alternatives since in both cases the shortest H···H distances are about 2.3 Å, approximately equal to twice the van der Waals radius of H. Similarly, the hydrogen-bond networks are equivalent for both alternatives and can therefore not provide an argument to prefer one over the other. However, an angle between CuN1 axes (~g_1 principal axes) of neighboring molecules has been calculated above from exchange effects in the EPR spectrum. As will be shown this angle allows us to distinguish between the two alternatives for constructing ordered hydrogen-bonded layers. Remember that the angle was obtained assuming exchange between two sites (out of four) without specifying which two sites. In the light of the molecular packing this prerequisite for a simple interpretation of the observed g values may be made more precise: we assume exchange averaging *within* layers via hydrogen bonds to be stronger than *between* layers via H···H van der Waals contacts thereby implying that the angle obtained from the EPR spectrum expresses the relative orientation of molecules in the same layer. For the two alternatives of ordered layers described above angles of 32 and 65°, respectively, are calculated. The agreement of the latter value with the value of 61 (4)° from the EPR spectrum leads us to conclude that molecules in an ordered layer are likely to be related by an *a* glide plane perpendicular to *c*.

Probable Nature of the Low-Temperature Structure of $Cu(tach)_2(NO_3)_2$. The crystal we investigated could be cooled and warmed between 4 and 300 K without shattering. This observation, together with the fact that the orientation of principal axes of the low-temperature **g** tensor almost coincides with CuN directions at room temperature, indicates that the packing of $Cu(tach)_2^{2+}$ cations and NO_3^- anions (Figure 1) is not severely changed during the phase transition at about 120 K. Thus at all temperatures $Cu(tach)_2(NO_3)_2$ is arranged in layers extending in the *bc* plane. Within layers $Cu(tach)_2^{2+}$ ions with C_{2h} symmetry and NO_3^- anions with C_s symmetry are held together via hydrogen bonds. Successive layers are held together by weak H···H van der Waals contact. Except for symmetry the packing is very similar to that of $Cu(tach)_2(ClO_4)_2$.

The occurrence of two different sites at low temperature, as deduced from EPR spectroscopy, is incompatible with the molecular C_{2h} symmetry required by the space group found at room temperature ($C2/m$). Removal of this symmetry, i.e., of the twofold axes and mirror planes would leave 2_1 axes parallel to *b* and *a* glide planes perpendicular to *b* corresponding to $P2_1/a$ (with *b* as unique axis) as a possible space group of the low-temperature structure. For such a structure all $Cu(tach)_2^{2+}$ ions in the same layer are still related by

translation, i.e., they show the same orientation of their **g** tensors, whereas molecules in successive layers show different orientation of **g** tensors. If we assume—as we did for the perchlorate salt—that magnetic exchange interactions tend to be stronger within layers than between layers, the proposed structure is compatible with the observed EPR spectrum showing two chemically equivalent but distinguishable Cu sites with no exchange interaction between the two. Other models with more complicated stacking of layers and involving varying degrees of disorder would also be compatible with the EPR data.

3.3. Angular Potential Parameters. $Cu(tach)_2(ClO_4)_2$. Due to the complication caused by intermolecular exchange couplings, no detailed experimental information on $V(\phi)$ could be obtained. From the static nature of the Jahn–Teller distortion as observed by X-ray crystallography and from the anisotropy of the powder EPR spectrum at room temperature, it can only be deduced that the lowest angular minimum is separated from possible other minima by at least 200 cm^{-1}.

$Cu(tach)_2(NO_3)_2$. Here the EPR results give considerably more information on the temperature-dependent shape of the angular potential $V(\phi)$. Below 120 K, all CuN_6 octahedra are elongated along the Cu–N1 direction; therefore the corresponding angular minimum is situated at least 100 cm^{-1} below any other minimum. A potential energy diagram which accounts for this and for the presence of two equivalent sites with a slight orthorhombic distortion is given in Figure 3c. The average **g** tensor observed immediately above the transition temperature can be explained by assuming that the CuN_6 octahedra are elongated almost exclusively along the two other axes, Cu–N2 and Cu–N2′; in principle the averaging could be due either to magnetic exchange coupling between statically distorted $Cu(tach)_2^{2+}$ clusters or to partially dynamic (sd or "planar dynamic"[56]) behavior, i.e., to fast thermal transitions ($\gtrsim$1 GHz) between the two energetically equivalent minima. In view of the available evidence for other CuL_6 complexes[24] we favor the latter alternative. In any case the angular potential appropriate for the description of individual $Cu(tach)_2^{2+}$ ions in the low-temperature region (Figure 3) is modified at high temperatures, presumably due to cooperative structural changes associated with the phase transition: above 120 K the Cu–N1 minimum is approximately 100 cm^{-1} higher than the two equivalent minima corresponding to elongation along Cu–N2 and Cu–N2′, respectively (Figure 3b). Finally, the gradual decrease of the **g** tensor anisotropy upon further warming from 120 to 300 K indicates that the thermal population of all three Cu–N elongations is more and more equalized at higher temperatures and that transitions occur between all angular minima at a rate sufficient to result in complete averaging of the EPR spectra.[24] This interpretation is consistent with the room-temperature X-ray result; the residual imbalance of thermal population of states along the angular potential at room temperature reflected from the small g anisotropy (last row in Table XI) is not sufficiently large for a detectable influence on the structural and thermal motion parameters measured by X-ray diffraction.

While the above simple picture in terms of thermal averaging of three mutually perpendicular tensors (with principal values found at 4 K) explains the gross features of the temperature dependence of the EPR spectra, there is no doubt that the actual situation is more complex. The observed rotation of the g axes in the monoclinic plane proves clearly that the angular potential between 120 and 300 K does not have the idealized shape shown in Figure 3b. There are, for example, no symmetry requirements to force the two symmetry-equivalent minima to be situated exactly at $\phi = 2\pi/3$ and $4\pi/3$; also variations of $V(\phi)$ with temperature cannot be ruled out.

4. Comparison of Structural and Spectroscopic Properties of $Cu(tach)_2^{2+}$ with Those of Other Octahedral CuN_6 Complexes

From the structural comparison of Cu(II) complexes with octahedral CuN_6 chromophores (Table X), we concluded that the scatter of d_0 and R_{JT} for a given chromophore caused by different lattice environments and experimental uncertainties is larger than the differences between values for different chromophores.

In order to check whether the approximate invariance found for the Jahn–Teller radii of CuN_6 complexes (Table X) also holds for the related spectroscopic quantities, we compare in Table XII five observables, d_0, R_{JT}, E_{JT} ($\approx\Delta E_1/4$), ΔE_2 ($\approx\Delta + 2E_{JT}$), and g_{iso} (which depend only to a minor extent on angular Jahn–Teller potential parameters), and two derived quantities, k and f. The quantity k is the average covalency reduction factor defined in eq 16 and f is the harmonic force constant for the radial part of the Jahn–Teller-active Cu–N stretching vibration defined in eq 5. The force constants f for the five different CuN_6 chromophores considered have a better chance to remain approximately constant than $h\nu$ or a which also depend on effective mass. In Table XII only undiluted solids with known crystal structures are included; spectroscopic data from liquid or frozen solutions and from diluted solids are omitted because for these no unambiguous correlation to structural properties is possible.

Inspection of Table XII shows that all seven quantities considered are very similar for the whole series of CuN_6 complexes. It is therefore meaningful to include average values and standard deviations which are added at the bottom of Table XII. As expected, the average copper–nitrogen bond lengths d_0 are somewhat larger for the aliphatic sp^3-type nitrogen donors (tach and en) than for the sp^2-type nitrogen donors (bpy, phen, and NO_2^-). The calculated standard deviations for all quantities except d_0 are of the same order of magnitude as the experimental uncertainty for individual values. There is no obvious correlation between variations in spectroscopic and structural quantities and the averages of k and f (0.627, 0.79 mdyn/Å) agree with k and f obtained from averaged R_{JT}, E_{JT}, ΔE_2, and g_{iso} (0.629, 0.77 mdyn/Å; eq 5 and 16). We therefore conclude that at present the *average* values of the quantities in Table XII describe CuN_6 chromophores equally well as corresponding R_{JT}, E_{JT}, ΔE_2, g_{iso}, k, and f of *individual* compounds.

The values of k and f and their approximate constancy in our series of compounds deserve a special comment. For pure σ-donor ligands (en, tach) the observed deviation of k from unity should be caused almost enitrely by σ covalency (eq 17) while in the case of potential π-acceptor ligands (bpy, phen, NO_2^-) π-covalency terms could also contribute.[43] There are two possible explanations for the observed insensitivity of k (and also of g_{iso} and ΔE_2) to variations in the type of ligand: either the σ covalency of the former set of complexes (placing approximately one-third of the e_g orbital density on the ligands) is decreased in the latter set and compensated by an equal amount of π covalency or else the σ covalency is almost constant throughout the series and π terms play a relatively unimportant role. Because explanations that involve "accidental cancellations" are seldom convincing, we favor the latter alternative.

Due to its R_{JT}^{-2} dependence, the effective force constant $f(e_g)$ for the corresponding Cu–N stretching vibrations has by far the largest relative standard deviation of all quantities in Table XII. Nevertheless the calculated value of 0.79 ± 0.14 mdyn/Å compares favorably with the value of 0.71 for $Ni(NH_3)_6^{2+}$ determined directly from Raman spectroscopy[64] and is in agreement with the predictions of the harmonic first-order Jahn–Teller model where f is taken to be identical with the

Table XII. Correlation of Structural and Spectroscopic Data of Crystalline Cu(II) Complexes with Six Chemically Equivalent Nitrogen Ligands in the First Coordination Sphere

complex[a]	T,[j] K	d_0, Å	R_{JT},[b] Å	E_{JT},[c] $cm^{-1} \times 10^3$	ΔE_2,[d] $cm^{-1} \times 10^3$	g_{iso}[e]	k[f]	f[g]
$Cu(tach)_2(ClO_4)_2$[h,41]	RT	2.167	0.328 s	2.20	15.75	2.12_1	0.61	0.81
$Cu(tach)_2(NO_3)_2$[h]	RT	2.164	0.329 d			2.13_2		0.80
$Cu(en)_3SO_4$[33,62]	RT	2.150	0.358 d	2.18	15.70	2.115	0.57	0.68
	4		s	2.05	16.6	2.115	0.60	
$Cu(bpy)_3(ClO_4)_2$[37]	RT	2.134	0.355 s	2.17	15.4	2.127	0.63	0.69
$Cu(phen)_3(ClO_4)_2$[37]	RT	2.134	0.336 s	1.90	15.2	2.134	0.65	0.67
$K_2PbCu(NO_2)_6$[22a,26,61]	RT	2.111	0.333 d	1.75	16.5	2.125	0.65	0.63
	RT	2.114	0.284 d					
	160		s	1.80	16.5	2.11_8	0.62	0.86
$Tl_2PbCu(NO_2)_6$[22a,26]	RT	2.118	0.308 d					(0.78)
	77			1.86	16.5	2.12_0	0.65	
$Rb_2PbCu(NO_2)_6$[22a,26,61,63]	RT	2.136	0.252 sd	1.92	15.7	2.127	0.63	1.20
	160		s	1.92	16.3	2.12_1	0.63	
$Cs_2PbCu(NO_2)_6$[25,61]	RT	2.171	0.343 sd					(0.75)
	160		s	2.22	16.0	2.12_1	0.62	
$K_2CaCu(NO_2)_6$[26]	RT	2.138	0.303 s	1.98	16.50			0.85
	77		s			2.123	(0.64)	
$K_2SrCu(NO_2)_6$[26]	RT	2.127	0.318 s	1.90	16.5			0.75
	77		s			2.12	(0.65)	
$K_2BaCu(NO_2)_6$[26]	RT	2.132	0.308 s	1.92	16.55			0.81
	77		s			2.12	(0.6_3)	
average values		2.138	0.320	1.98	16.12	2.123	0.627	0.79
standard deviation {	abs value	0.019	0.029	0.15	0.48	0.005[i]	0.023	0.14
	in %	0.9	9.0	7.5	3.0	4[i]	3.7	18

[a] References for optical and EPR data only. References for structural data are given in Table X. [b] Jahn–Teller radii as defined in eq 8 and 9, from Table X: s = static, d = dynamic, sd = partially dynamic. [c] Jahn–Teller energy calculated from first electronic d–d transition using $\Delta E_1 = 4E_{JT}$ (eq 7). [d] Average $(xy, yz, zx) \leftarrow (x^2 - y^2)$ excitation energy (eq 8). [e] Average g value $g_{iso} = {}^1/_3(g_x + g_y + g_z)$. [f] Average combined spin–orbit and orbital angular momentum reduction factor defined by $g_{iso} - 2.0023 = (4u - 5u^2)$ with $u = k\zeta/(\Delta E_2)$ and $\zeta = 826\ cm^{-1}$. If g_{iso} and ΔE_2 have been measured at different temperatures, k values are put in parentheses. [g] Force constant for the Jahn–Teller active degenerate Cu–N stretching vibration in mdyn/Å calculated by using $f = 2E_{JT}/R^2_{JT}$ (eq 5). [h] This work. [i] Standard deviation for the average g shift $\Delta g_{iso} = g_{iso} - 2.0023$. [j] RT = room temperature.

value expected for a hypothetical octahedral CuN_6 complex without Jahn–Teller effect (eq 3). As expected, $f(e_g)$ is substantially smaller than the Raman value of $f(a_{1g}) \approx 1.8$ mdyn/Å for the totally symmetric Cu–N breathing mode of strongly tetragonally elongated $Cu(NH_3)_4X_2$ complexes.[64-66]

5. Summary and Conclusion

In order to derive information on the Born–Oppenheimer energy surface of Jahn–Teller-active trigonal Cu(II) complexes with CuN_6 chromophores, the complex cation $Cu(tach)_2^{2+}$ (tach = *cis,cis*-1,3,5-triaminocyclohexane) was investigated in two different solids, $Cu(tach)_2(NO_3)_2$ and $Cu(tach)_2(ClO_4)_2$, by X-ray crystallography at room temperature and by EPR spectroscopy between 4 and 300 K. The structure of Jahn–Teller-inactive $Ni(tach)_2(NO_3)_2$ was also determined for comparison.

The *structure determination* of the perchlorate salt revealed that the CuN_6 octahedron shows static tetragonal elongation at room temperature. In the nitrate salt, $Cu(tach)_2^{2+}$ is very likely to undergo purely dynamic Jahn–Teller distortion, in spite of its low (C_{2h}) site symmetry. The amplitude of this distortion was estimated from the observed temperature factors of $Cu(tach)_2(NO_3)_2$ and $Ni(tach)_2(NO_3)_2$ by two methods. Both methods, namely, semirigid body analysis of the entire complex cation $M(tach)_2^{2+}$ and analysis of differences in thermal motion between Cu, Ni, and N, lead essentially to the same value (0.33 Å) for the Jahn–Teller radius R_{JT}. Furthermore both R_{JT} and the average Cu–N distance d_0 were found to be equal within experimental error for dynamically distorted $Cu(tach)_2(NO_3)_2$ and statically distorted $Cu(tach)_2(ClO_4)_2$.

By *variable-temperature EPR analysis*, $Cu(tach)_2(ClO_4)_2$ was found to be statically distorted in the whole range between 4 and 300 K, while $Cu(tach)_2(NO_3)_2$ showed a gradual transition from static to dynamic behavior: below ~120 K the CuN_6 chromophore shows static elongation along the Cu–N1 axis (Figure 13); at ~120 K a phase transition leads to a structure in which dynamic oscillation between two static elongations along the equivalent Cu–N2 and Cu–N2′ takes place (sd or "planar dynamic JTE"[56]). At still higher temperatures (120–300 K) the dynamic Jahn–Teller motion becomes more and more isotropic. From the EPR data approximate information on the nature of the low-temperature crystal structures and on the *angular* shape of the Mexican hat potential $E_{el}(|S_2|,\phi)$ could be obtained.

The optical and EPR data of Childers, Wentworth, and Zompa[41] and the present X-ray and EPR results for $Cu(tach)_2^{2+}$ suggest that the average Cu–N distance d_0, the Jahn–Teller radius R_{JT}, the Jahn–Teller stabilization energy E_{JT}, the cubic ligand field splitting parameter Δ, the isotropic part of the g tensor, g_{iso}, the average spin–orbit and orbital momentum reduction factor k, i.e., the covalency parameters for the local CuN_6 chromophore, and the quadratic force constant f for the Jahn–Teller-active degenerate Cu–N stretching mode are almost unchanged by differences in molecular environment arising from the presence of different anions or from incorporation into diluted and undiluted lattices, respectively. The properties in question are more or less independent of the small details characterizing the angular part of the Mexican hat potential $E_{el}(|S_2|,\phi)$.

A comparison between $Cu(tach)_2^{2+}$ and $Cu(en)_3^{2+}$, $Cu(bpy)_3^{2+}$, $Cu(phen)_3^{2+}$, $Cu(NO_2)_6^{4-}$, i.e., between CuN_6 complexes with six chemically equivalent nitrogen atoms in different lattices, showed that the "nonangular" properties listed above are very similar in all cases; the following values and standard deviations were obtained from a total of 13 structural and spectroscopic investigations: Jahn–Teller energy (eq 7), $E_{JT} = 0.20 \pm 0.02\ \mu m^{-1}$; Jahn–Teller radius (eq 9, 10), $R_{JT} = 0.32 \pm 0.03$ Å; average Cu–N distance, $d_0 = 2.14 \pm 0.02$ Å; cubic ligand field splitting (eq 8), $\Delta = (12.1 \pm 0.5)$

$\times 10^3$ cm^{-1}; average g value (eq 18), $g_{iso} = 2.123 \pm 0.005$; average covalency factor (eq 16), $k = 0.63 \pm 0.03$; harmonic e_g force constant (eq 5), $f = 0.79 \pm 0.14$ mdyn/Å.

The above standard deviations are of the order of the experimental uncertainties and none of the above quantities differs significantly in statically and dynamically distorted systems. We therefore conclude that consideration of the local CuN_6 fragment alone (cluster model) suffices for an adequate description of the Jahn–Teller effect and of the metal–ligand bonding and that very similar radial Jahn–Teller potential parameters may be used for most CuN_6 complexes.

Finally, the present results also illustrate that the distinction between genuine and pseudo-Jahn–Teller effect often emphasized by spectroscopists loses much of its importance in systems with strong Jahn–Teller coupling.[3,12,38] Intermolecular forces typical for molecular crystals (and probably also for liquid solutions) do not affect the radial topology of the Mexican hat potential to a large extent; they merely produce modifications in the angular behavior.[70]

Acknowledgment. We thank the late Professor G. Schwarzenbach, Dr. W. Marty, and Dr. C. W. Schläpfer for discussion and for various samples, Professor D. Reinen for helpful comments on the manuscript, Professor K. N. Trueblood for the computer program used in the rigid and semirigid body analyses, Dr. F. K. Winkler for the constraint least-squares program, and Professor A. v. Zelewsky, Dr. C. W. Schläpfer, and Dr. C. Daul for the program used in the computer simulation of the EPR spectra. This work was supported by the "Schweizerischer Nationalfonds zur Förderung der wissenschaftlichen Forschung" under Projects 2.398-0.75 and 2.340-0.75.

Registry No. $Cu(tach)_2(ClO_4)_2$, 31220-63-0; $Cu(tach)_2(NO_3)_2$, 67722-61-6; $Ni(tach)_2(NO_3)_2$, 67722-62-7.

Supplementary Material Available: A listing of structure factor amplitudes (21 pages). Ordering information is given on any current masthead page.

References and Notes

(1) B. J. Hathaway and D. E. Billing, *Coord. Chem. Rev.*, **5**, 143 (1970).
(2) I. B. Bersuker, *Coord. Chem. Rev.*, **14**, 357 (1975).
(3) J. Gažo, I. B. Bersuker, J. Garaj, M. Kabešová, J. Kohout, H. Langfelderová, M. Melnik, M. Serátor, and F. Valach, *Coord. Chem. Rev.*, **19**, 253 (1976).
(4) W. Moffitt and W. Thorson, *Phys. Rev.*, **108**, 357 (1957).
(5) U. Oepik and M. H. L. Pryce, *Proc. R. Soc. London, Ser. A*, **238**, 425 (1957).
(6) H. C. Longuet-Higgins, U. Oepik, M. H. L. Pryce, and R. A. Sack, *Proc. R. Soc. London, Ser. A*, **244**, 1 (1958).
(7) H. A. Jahn and E. Teller, *Proc. R. Soc. London*, **161**, 220 (1937).
(8) J. D. Dunitz and L. E. Orgel, *J. Phys. Chem. Solids*, **3**, 20 (1957).
(9) M. C. M. O'Brien, *Proc. R. Soc. London, Ser. A*, **281**, 323 (1964).
(10) (a) F. S. Ham, *Phys. Rev. A*, **138**, 1727 (1965); (b) *Phys. Rev.*, **166**, 307 (1968).
(11) L. L. Lohr, Jr., *Inorg. Chem.*, **6**, 1890 (1967).
(12) M. D. Sturge, *Solid State Phys.*, **20**, 91 (1968).
(13) R. Englman, "The Jahn-Teller Effect in Molecules and Crystals", Wiley, New York, N.Y., 1972.
(14) R. E. Coffman, *J. Chem. Phys.*, **48**, 609 (1968).
(15) W. Low and J. T. Suss, *Phys. Lett.*, **7**, 310 (1963).
(16) R. E. Coffman, D. L. Lyle, and D. R. Mattison, *J. Phys. Chem.*, **72**, 1392 (1968).
(17) R. G. Wilson, F. Holnj, and N. E. Hedgecock, *Phys. Rev. B*, **1**, 3609 (1970).
(18) R. H. Borcherts, A. Kanzaki, and H. Abe, *Phys. Rev. B*, **2**, 23 (1970).
(19) S. Guha and L. L. Chase, *Phys. Rev. Lett.*, **32**, 869 (1974).
(20) F. S. Ham in "Electron Paramagnetic Resonance", S. Geschwind, Ed., Plenum Press, New York, N.Y., 1972.
(21) N. Gauthier and M. B. Walker, *Phys. Rev. Lett.*, **31**, 1211 (1973).
(22) (a) J. Grefer und D. Reinen, *Z. Naturforsch., A*, **28**, 464 (1973); (b) D. Reinen und H. Weitzel, *Z. Anorg. Allg. Chem.*, **424**, 31 (1976).
(23) B. Bleaney, K. D. Bowers, and R. Trenam, *Proc. R. Soc. London, Ser. A*, **228**, 157 (1955).
(24) D. Getz and B. L. Silver, *J. Chem. Phys.*, **61**, 638 (1974).
(25) D. Reinen, *Solid State Commun.*, **21**, 137 (1977).
(26) D. Reinen, C. Friebel, and K. P. Reetz, *J. Solid State Chem.*, **41**, 103 (1972).
(27) P. S. Rao and S. Subramanian, *J. Magn. Reson.*, **22**, 191 (1976).
(28) B. Nieuwenhuijse and J. Reedijk, *Chem. Phys. Lett.*, **22**, 201 (1973).
(29) D. L. McFadden, A. T. McPhail, C. D. Garner, and F. E. Mabbs, *J. Chem. Soc., Dalton Trans.*, 263 (1975).
(30) D. L. Cullen and E. C. Lingafelter, *Inorg. Chem.*, **9**, 386 (1970).
(31) T. S. Piper and A. G. Karipides, *Inorg. Chem.*, **4**, 923 (1965).
(32) L. N. Swink and M. Atoji, *Acta Crystallogr.*, **13**, 639 (1970).
(33) I. Bertini, D. Gatteschi, and A. Scozzafava, *Inorg. Chem.*, **16**, 1973 (1977).
(34) C. K. Jørgensen, *Acta Chem. Scand.*, **9**, 1362 (1955).
(35) R. A. Palmer and T. S. Piper, *Inorg. Chem.*, **5**, 864 (1966).
(36) G. F. Kokoszka, C. W. Reimann, H. C. Allen, Jr., and G. Gordon, *Inorg. Chem.*, **6**, 1657 (1967).
(37) (a) B. J. Hathaway, M. J. Bew, D. E. Billing, R. J. Dudley, and P. Nicholls, *J. Chem. Soc. A*, 2312 (1969); (b) B. J. Hathaway, P. G. Hodgson, and P. C. Power, *Inorg. Chem.*, **13**, 2009 (1974).
(38) J. Pradilla-Sorzano and J. P. Fackler, Jr., *Inorg. Chem.*, **12**, 1182 (1973), and references therein.
(39) (a) R. C. Koch, J. H. Venable, and M. D. Joesten, *J. Chem. Phys.*, **51**, 6312 (1973); (b) R. A. Palmer and C. R. Taylor, *Inorg. Chem.*, **10**, 2546 (1971).
(40) M. D. Joesten, M. S. Hussain, and P. G. Lenhert, *Inorg. Chem.*, **9**, 151 (1970).
(41) R. F. Childers, R. A. D. Wentworth, and L. J. Zompa, *Inorg. Chem.*, **10**, 302 (1971).
(42) A. Abragam and B. Bleaney, "Electron Paramagnetic Resonance of Transition Metal Ions", Clarendon Press, Oxford, 1970.
(43) B. R. Mc Garvey in "Electron Spin Resonance of Metal Complexes", Plenum Press, New York, N.Y., 1969, p 1.
(44) H. R. Buys and J. J. Geise, *Tetrahedron Lett.*, 2991 (1970); A. Yokozeki, K. Kuchitsu, and Y. Morino, *Bull. Chem. Soc. Jpn.*, **43**, 2017 (1970).
(45) P. Andersen and O. Hassel, *Acta Chem. Scand.*, **5**, 1349 (1951).
(46) (a) V. Schomaker and K. N. Trueblood, *Acta Crystallogr., Sect. B*, **24**, 63 (1968); (b) see, for example, J. L. Baudour, *Acta Crystallogr., Sect. B*, **28**, 1649 (1972); J. D. Dunitz and D. N. J. White, *Acta Crystallogr., Sect. A*, **29**, 93 (1973); E. Prince and L. W. Finger, *Acta Crystallogr., Sect. B*, **29**, 179 (1973); J. Sygusch, *Acta Crystallogr., Sect. B*, **32**, 3295 (1976).
(47) From Tables VI and VIII it may be seen that the transformation matrices from fractional coordinates (x, y, z) to inertial coordinates (X, Y, Z) of $M(tach)_2^{2+}$ and of tach alone are very similar; qualitative comparisons between vectors in different inertial systems are therefore meaningful. Furthermore, the motion of the metal is only translational because it sits on a center of symmetry, i.e., on the intersection of the three libration axes.
(48) Mazkar-Ul-Haque, C. N. Caughlan, and K. Emerson, *Inorg. Chem.*, **9**, 2421 (1970).
(49) O. P. Anderson, *J. Chem. Soc., Dalton Trans.*, 2597 (1972).
(50) O. P. Anderson, *J. Chem. Soc., Dalton Trans.*, 1237 (1973).
(51) N. W. Jsaacs and C. H. L. Kennard, *J. Chem. Soc. A*, 386 (1969).
(52) S. Takagi, M. D. Joesten, and P. G. Lenhert, *Acta Crystallogr., Sect. B*, **31**, 1968 (1975).
(53) D. L. Cullen and E. C. Lingafelter, *Inorg. Chem.*, **10**, 1264 (1971).
(54) S. Takagi, M. D. Joesten, and P. G. Lenhert, *Acta Crystallogr., Sect. B*, **32**, 326 (1976).
(55) S. Takagi, M. D. Joesten, and P. G. Lenhert, *Acta Crystallogr., Sect. B*, **32**, 1278 (1976).
(56) D. Mullen, G. Heger, and D. Reinen, *Solid State Commun.*, **17**, 1249 (1975).
(57) S. Takagi, M. D. Joesten, and P. G. Lenhert, *J. Am. Chem. Soc.*, **96**, 6603 (1974).
(58) S. Takagi, M. D. Joesten, and P. G. Lenhert, *Acta Crystallogr., Sect. B*, **32**, 2524 (1976).
(59) S. Takagi, M. D. Joesten and P. G. Lenhert, *Acta Crystallogr., Sect. B*, **31**, 596 (1975).
(60) S. Takagi, M. D. Joesten, and P. G. Lenhert, *Acta Crystallogr., Sect. B*, **31**, 1970 (1975).
(61) C. Friebel, *Z. Anorg. Allg. Chem.*, **417**, 197 (1975).
(62) R. Rajan and T. R. Reddy, *J. Chem. Phys.*, **39**, 1140 (1963).
(63) M. D. Joesten, S. Takagi, and J. H. Venable, Jr., *Chem. Phys. Lett.*, **36**, 536 (1975).
(64) K. H. Schmidt and A. Müller, *Coord. Chem. Rev.*, **19**, 41 (1976).
(65) B. N. Cyvin, S. J. Cyvin, K. H. Schmidt, W. Wiegeler, A. Müller, and J. Brunvoll, *J. Mol. Struct.*, **30**, 315 (1976).
(66) R. Dudley, B. J. Hathaway, P. G. Hodgson, J. K. Mulcahy, and H. A. G. Tomlinson, *J. Inorg. Nucl. Chem.*, **36**, 1947 (1974).
(67) "International Tables for X-Ray Crystallography", Vol. III, The Kynoch Press, Birmingham, England, 1968.
(68) D. Cromer and J. Mann, *Acta Crystallogr., Sect. A*, **24**, 321 (1968).
(69) R. F. Stewart, E. R. Davidson, and W. T. Simpson, *J. Chem. Phys.*, **42**, 3175 (1965).
(70) After completion of the manuscript, D. Reinen kindly communicated to us Cu–N bond distances for $Cs_2PbCu(NO_2)_6$ (2.07, 2.11, and 2.30 Å; S. Kline and D. Reinen, in press) and for γ-$K_2PbCu(NO_2)_6$ (2.04, 2.05, and 2.23 Å; Y. Noda, M. Mori, and Y. Yamada, unpublished work).